THE COSMIC EVOLUTION SURVEY (COSMOS): SUBARU OBSERVATIONS OF THE HST COSMOS FIELD [1]

Y. Taniguchi [2], N. Scoville [3,4], T. Murayama [5], D. B. Sanders [6], B. Mobasher [7], H. Aussel [8], P. Capak [3], M. Ajiki [5], S. Miyazaki [9], Y. Komiyama [10], Y. Shioya [2], T. Nagao [10,11], S. S. Sasaki [2,3,5], J. Koda [3], C. Carilli [12], M. Giavalisco [13], L. Guzzo [14], G. Hasinger [15], C. Impey [16], O. LeFevre [17], S. Lilly [18], A. Renzini [19], M. Rich [20], E. Schinnerer [21], P. Shopbell [3], N. Kaifu [10], H. Karoji [10], N. Arimoto [10], S. Okamura [22], and K. Ohta [23]

---

[1]Based on data collected at Subaru Telescope, which is operated by the National Astronomical Observatory of Japan.

[2]Physics Department, Graduate School of Science & Engineering, Ehime University, 2-5 Bunkyo-cho, Matsuyama 790-8577, Japan

[3]California Institute of Technology, MC 105-24, 1200 East California Boulevard, Pasadena, CA 91125

[4]Visiting Astronomer, University of Hawaii, 2680 Woodlawn Drive, Honolulu, HI, 96822

[5]Astronomical Institute, Graduate School of Science, Tohoku University, Aramaki, Aoba, Sendai 980-8578, Japan

[6]Institute for Astronomy, 2680 Woodlawn Drive, University of Hawaii, Honolulu, HI, 96822

[7]Space Telescope Science Institute, 3700 San Martin Drive, Baltimore, MD 21218

[8]Service d'Astrophysique, CEA/Saclay, 91191 Gif-sur-Yvette, France

[9]Subaru Telescope, National Astronomical Observatory, 650 N. A'ohoku Place, Hilo, HI 96720, USA

[10]National Astronomical Observatory of Japan, 2-21-1 Osawa, Mitaka, Tokyo 181-8588, Japan

[11]INAF – Osservatorio Astrofisico di Arcetri, Largo Enrico Fermi 5, 50125 Firenze, Italy

[12]National Radio Astronomy Observatory, P.O. Box 0, Socorro, NM 87801-0387

[13]Space Telescope Science Institute, 3700 San Martin Drive, Baltimore, MD 21218

[14]Osservatorio Astronomico di Brera, via Brera, Milan, Italy

[15]Max Planck Institut fuer Extraterrestrische Physik, D-85478 Garching, Germany

[16]Steward Observatory, University of Arizona, 933 North Cherry Avenue, Tucson, AZ 85721

[17]Laboratoire d'Astrophysique de Marseille, BP 8, Traverse du Siphon, 13376 Marseille Cedex 12, France

[18]Department of Physics, Swiss Federal Institute of Technology (ETH-Zurich), CH-8093 Zurich, Switzerland

[19]European Southern Observatory, Karl-Schwarzschild-Str. 2, D-85748 Garching, Germany

[20]Department of Physics and Astronomy, University of California, Los Angeles, CA 90095

[21]Max Planck Institut für Astronomie, Königstuhl 17, Heidelberg, D-69117, Germany

[22]Department of Astronomy, Graduate School of Science, The University of Tokyo, 7-3-1 Hongo, Bunkyo-ku, Tokyo 113-0033, Japan

[23]Department of Astronomy, Graduate School of Science, Kyoto University, Kitashirakawa, Sakyo-ku, Kyoto 606-8502, Japan

ABSTRACT

We present deep optical imaging observations of 2 square degree area, covered by the Cosmic Evolution Survey (COSMOS), made by the prime-focus Camera (Suprime-Cam) on the 8.2m Subaru Telescope. Observations were done in six broad-band [B (4459.7 Å), g' (4723.1 Å), V (5483.8 Å), r' (6213.0 Å), i' (7640.8 Å), z' (8855.0 Å)], and one narrow-band ($NB816$) filters. A total of 10^6 galaxies were detected to $i' \sim 26.5$ mag. These data, combined with observations at u^* and K-band are used to construct the photometric catalogs for the COSMOS and to measure their photometric redshifts, multi-band spectral energy distributions, stellar masses and identification of high redshift candidates. This catalog provides multi-waveband data for scientific analysis of the COSMOS survey.

Subject headings: galaxies: evolution — galaxies: interaction

1. INTRODUCTION

The Cosmic Evolution Survey (COSMOS) is a treasury program on the Hubble Space Telescope (HST), awarded a total of 640 HST orbits, carried out in two cycles (320 orbits in cycles 12 and 13 each; Scoville et al. 2006a; Koekemoer et al. 2006). COSMOS is a 2 square degree imaging survey of an equatorial field in I_{814} band, using the Advanced Camera for Surveys (ACS). The HST ACS observations provide high resolution imaging to map the morphology of galaxies as a function of environment and epoch covering from high redshift ($z \sim 6$) to the nearby ($z \sim 0$) universe. Since substantial large-scale structures (e.g., voids, filaments, groups and clusters of galaxies) occur on scales up to 100 Mpc in the comoving frame, our 2 square degree COSMOS field can adequately map galaxy evolution over the full range of environments[1]. It is also interesting to note that our survey volume at high redshift is similar to that of the Sloan Digital Sky Survey (York et al. 2000) at low redshift.

Our ACS survey depth, $I_{814,\rm lim} \simeq 27$ AB allows us to detect of the order of $\sim 10^6$ sources in the COSMOS area. Therefore, the COSMOS project is fundamental to virtually all areas of galaxy evolution, identification of different classes of objects, evolution of large-scale structures as well as that of dark matter. In particular, the following interesting issues can be covered by our COSMOS project using statistically large samples: [1] the evolution of galaxies, clusters, large-scale structure, and cold dark matter on mass scales up to $> 10^{14} M_\odot$ as a function of redshift, [2] the formation, assembly, and evolution of galaxies as a function of large-scale structure environment, morphology

[1]Note that 1.4 degree corresponds to a co-moving scale of 46.1 Mpc for $z = 0.5$, 80.7 Mpc for $z = 1$, 126.6 Mpc for $z = 2$, 155.3 Mpc for $z = 3$, 175.2 Mpc for $z = 4$, 190.0 Mpc for $z = 5$, and 201.5 Mpc for $z = 6$, under a flat cosmology of $\Omega_\Lambda = 0.7$, $\Omega_{\rm m} = 0.3$, and $H_0 = 70$ km s^{-1} Mpc^{-1}.

and redshift, [3] the cosmic star formation history as a function of large-scale structure environment, morphology and redshift, and [4] detailed study of the nature, morphology and clustering properties of different populations of galaxies such as active galactic nuclei (AGNs), extremely red objects, Lyα emitters (LAEs), Lyman Break Galaxies (LBGs), and star-forming galaxies, and their evolution with redshift.

However, to understand the whole evolution of galaxies, AGNs, and dark matter, it is absolutely necessary to obtain multi-wavelength observations with high spatial resolution from X-ray to radio. In particular, we need optical multi-band images of the COSMOS field, as we only take I_{814} band data with ACS. Therefore, ground-based optical observations are also an essential part of the COSMOS project. Such data will be helpful in studying stellar contents of one million galaxies at various redshifts and in estimating photometric redshifts with reasonable accuracy. This could best be accomplished by using wide-area CCD detectors on 8m class telescopes. In this respect, the Subaru Prime-Focus Camera, Suprime-Cam (Miyazaki et al. 2002), on the Subaru Telescope (Kaifu et al. 2000; Iye et al. 2004), provides its superior imaging capability because of its very wide field of view ($34' \times 27'$).

During the period January 2004 to April 2005, we obtained deep optical images of the COSMOS field with Suprime-Cam with the following seven filters; B, g', V, r', i', z', and $NB816$. We describe these observations in detail; see also Taniguchi et al. (2005). The last filter is the narrowband filter centered at 815 nm with a FWHM of 12 nm. The broad-band data will be used to measure photometric redshifts and stellar mass (Mobasher et al. 2006), identify large scale structures (Scoville et al. 2006b; Guzzo et al. 2006), estimate local densities (Capak et al. 2006b) and optically identify sources detected in X-ray (Hasinger et al. 2006), radio (Schinnerer et al. 2006), and infrared (Sanders et al 2006) wavelengths. Combined with the narrow-band (NB816) observations, these will be used to identify LAEs at $z = 5.7$ (Murayama et al 2006), [O II] emitters at $z = 1.2$ (Takahashi et al. 2006), and Hα emitters at $z = 0.24$ (Shioya et al. 2006).

In the present paper we describe in detail the observational procedures, filters, sensitivities and completeness of the COSMOS Subaru Suprime-Cam imaging (see also Taniguchi et al. 2005). Science investigations and their initial results are presented in the aforementioned papers. Throughout this paper, we use the AB magnitude system.

2. OBSERVATIONS

2.1. Observational Strategy

The COSMOS field covers an area of 1.4 × 1.4 degree, centered at RA(J2000) = 10:00:28.6 and DEC(J2000) = +02:12:21.0. The Suprime-Cam consists of ten 2048×4096 CCD chips and provides a very wide field of view, $34' \times 27'$ in 10240×8192 pixels ($0\farcs202$ pixel^{-1}). Despite the large field of view of the Supreme-Cam, we need a total of nine pointings to cover the whole COSMOS area.

This requires special mapping (i.e. dithering) patterns to carry out the imaging observations. In order to obtain accurate astrometry, we also need to arrange the patterns to overlap. Furthermore, we need to take care of gaps ($3''$–$4''$ or $16''$–$17''$) between the CCD chips of the Suprime-Cam. In order to save observing time, we need an efficient mapping pattern with minimum pointings for covering the whole field of COSMOS with minimizing the shallower edges around the outside of the mosaic. On one hand, in order to achieve reliable astrometry covering the whole COSMOS field, it is also necessary to have a half-array shifted data set.

Taking these two points into account, we use the following two mapping patterns; Pattern A and Pattern C. Originally, we had another Pattern B. However, we did not use this in our observations. From this historical reason, we refer our two mapping patterns as Pattern A and C throughout this paper. Pattern A is a half-array shifted mapping method in which 12 pointings are necessary to map the whole COSMOS field; see Figure 1. The detailed dithering properties are given in Table 1. Pattern C is our most efficient mapping method in which only nine pointings are enough to map the whole field; see Figure 2. The detailed dithering properties are given in Table 2. Pattern A was used with a relatively short unit exposure time (e.g., a few to several minutes) because this pattern data were used to obtain better astrometry and photometry in the whole COSMOS field (Aussel et al. 2006; Capak et al. 2006a). On the other hand, Pattern C was used with a longer unit integration time because this pattern was used to obtain deeper data efficiently.

2.2. Observational Programs and Runs

Our Suprime-Cam observations of the COSMOS field have been made during a period between 2004 January and 2005 March, consisting of three common-use observing programs. Four nights were allocated within the University of Hawaii observing time on the Subaru Telescope during a period between 2004 Feb and 2004 March; PI = N. Scoville. A summary of the observational programs is given in Table 3. It is noted that the two programs, S03B-239 and S04B-142, were allocated as an Open Use Intensive Program; such Intensive Programs provide the opportunity for researchers to proceed with large programs of advanced study that can only be achieved with the unique capability of Subaru Telescope and its instruments and needs an allocation of significant telescope time. Another Intensive Program (COSMOS-21) was also accepted in the semester S05B (S05B-013); note that '21" means 21 filters in the optical window. However, details of observations of S05B-013 will be given in a forthcoming paper.

Including the University of Hawaii time, 24.5 nights were allocated in total for our Suprime-Cam imaging of the COSMOS field. These observations were carried out in eight observing runs; see Table 4. During these runs, we obtained optical images of the COSMOS field with the Johnson broad band filters, B and V, the SDSS broad band filters, g', r', i', and z', and a narrowband

filter, $NB816$[2]. The filter response curves including the CCD sensitivity and the atmospheric transmission are shown in Figure 3.

3. DATA REDUCTION AND SOURCE DETECTION

3.1. Data Reduction

All the individual CCD data were reduced using IMCAT[3] by the standard process; bias subtraction, flat fielding, combining the frames, astrometry, and photometry. Here we note that the night sky subtraction needs two steps to account for fringing and scattered light. The scattered light also makes it difficult to carry out accurate flat fielding. However, our careful experiments show that the central $26'$ area of the field of view is stable at flat to 1% although the scattered light pattern shows variations as large as a few % outside the central $26'$ area. Details of these reduction procedure are described in Capak et al. (2006a) and Aussel et al. (2006). The PSF sizes of final images are summarized in Table 5. Note that the PSF size of the images used for generating the official catalogue was matched to that for the image with worst seeing ($1\farcs6$).

In Figure 4, we show the composite color image of the whole COSMOS field made from B, r', and z' data. The reduced images were divided into tiles with a dimension of $10' \times 10'$ as shown in Figure 5. Note that the center position of the COSMOS field is located in the #65 tile. The region colored in light-blue covered by 81 (9×9) tiles is the COSMOS HST/ACS field.

We estimate the limiting magnitudes by using the 81 tiles. For each tile, we performed aperture photometry for 10000 random points (810000 points in total) on the PSF matched image ($1\farcs6$) with $2''$ diameter and $3''$ diameter. Then we evaluated the limiting magnitudes from the standard deviation for the distribution of the random photometry. The results are summarized in Table 5. As shown in Table 5, the 3σ limiting magnitudes are deeper than 27 mag. ($2''$ aperture) in B, g', V, and r'. However, in z' band, the limiting magnitude reaches to 25.7 mag. Difference of the limiting magnitudes among the 81 tiles is less than 0.25 mag in each band (Figures 6–12).

Note that another type of limiting magnitudes can be estimated by using background limited numbers. These results are also shown in Figures 13–19 provided by Capak et al. (2006a; see their Table 4).

---

[2]Our SDSS broad-band filters are designated as g^+, r^+, i^+, and z^+ in Capak et al. (2006a) to distinguish from the original SDSS filters. Also, our B and V filters are designated as B_J and V_J in Capak et al. (2006) where J means Johnson and Cusins filter system used in Landolt (1992).

[3]IMCAT is distributed by Nick Keiser at http://www.ifa.hawaii.edu∼kaiser/imcat/

3.2. Source Detection and Completeness

In Figures 20 and 21 we show the number counts of detected objects against the magnitude measured with $2''$ aperture and $3''$ aperture for each band, respectively. In this analysis, we use SExtractor version 2.3.2 (Bertin & Arnouts 1996) with the detection criteria of 5-pix connection above the 2σ significance and measured aperture magnitude for the detected objects. The SExtractor parameter setup file used in our analysis is given in Table 6. Apparently, the source detection comes to be incomplete at a shallower magnitude than the limiting magnitude. This may be interpreted as a result of flux lost from extended sources. Note that breaks or drops of the number counts in the bright part are due to saturated objects.

In order to estimate detection completeness, we have performed a simulation using the IRAF ARTDATA. We assume that galaxies have two types of light distributions obeying the exponential law and the de Vaucouleurs' $r^{1/4}$ law. For each type of galaxies, we generated 200 model galaxies for each total magnitude interval (0.2 mag) in 9 tiles (#026, #029, #032, #062, #065, #068, #098, #101, and #104 in Figure 5). Their sky positions, half-light radius ($0\farcs15$ to $0\farcs75$), ellipticities (0.3 to 1.0), and position angles (0° to 360°) are randomly determined. Then these model galaxies are put into the CCD data together with Poisson noises. After smoothing model-galaxy images to match to the seeing size, we try to detect them using SExtractor with the same procedure as that used before. The detectability of the model galaxies in each band is shown in Figures 22–28 as a function of total magnitude and also summarized in Table 7.

In order to compare the input total magnitude of the model galaxies used in the completeness analysis with magnitudes obtained by aperture photometry, we measured the aperture magnitudes of them by SExtractor. Figures 29–32 show the relation between the aperture magnitude ($2''$ diameter and $3''$ diameter) and the input total magnitude of model galaxies with the profiles of the exponential law and de Vaucouleurs' law. The measured aperture magnitudes are always offset toward fainter against the input total magnitudes. These offsets are smaller for $3''$ aperture magnitudes.

3.3. Concluding Remarks

We present deep optical imaging observations made with the Suprime-Cam on the Subaru Telescope. Our observations cover the seven filter bands from B to z'. These imaging data allow us to investigate photometric properties of ~ 1 million galaxies found in the COSMOS field together with the high-resolution ACS I_{814} imaging data. The major COSMOS datasets including the Subaru images and catalogs are publicly available (following calibration and validation) through the web site for IPAC/IRSA:
`http://irsa.ipac.caltech.edu/data/COSMOS/`.

The HST COSMOS Treasury program was supported through NASA grant HST-GO-09822. We gratefully acknowledge the contributions of the entire COSMOS collaboration consisting of more than 70 scientists. More information on the COSMOS survey is available at `http://www.astro.caltech.edu/~cosmos`. It is a pleasure the acknowledge the excellent services provided by the NASA IPAC/IRSA staff (Anastasia Laity, Anastasia Alexov, Bruce Berriman and John Good) in providing online archive and server capabilities for the COSMOS datasets. The COSMOS Science meeting in May 2005 was supported in part by the NSF through grant OISE-0456439. We would also like to thank the staff at the Subaru Telescope for their invaluable help. In particular, we would like to thank Hisanori Furusawa because his professional help as a support scientist made our Suprime-Cam observations successful. This work was financially supported in part by the Ministry of Education, Culture, Sports, Science, and Technology (Nos. 10044052 and 10304013), and by JSPS (15340059 and 17253001). SSS and TN are JSPS fellows.

REFERENCES

Aussel, H., et al. 2006, ApJ, submitted

Bertin, E., & Arnouts, S. 1996, A&AS, 117, 393

Capak, P., et al. 2006a, ApJ, submitted

Capak, P., et al. 2006b, ApJ, submitted

Iye, M., et al. 2004, PASJ, 56, 381

Kaifu, N., et al. 2000, PASJ, 52, 1

Landolt, A. U. 1992, AJ, 104, 340

Miyazaki, S., et al. 2002, PASJ, 54, 833

Mobasher, B., et al. 2006, ApJ, submitted

Koekemoer, A., et al. 2006, ApJ, submitted

Murayama, T., et al. 2006, ApJ, submitted

Sasaki, S. S., et al. 2006, ApJ, submitted

Sanders, D. B., et al. 2006a, ApJ, submitted

Scoville, N. Z., et al. 2006a, ApJ, submitted

Scoville, N. Z., et al. 2006b, ApJ, submitted

Shioya, Y., et al. 2006, ApJ, submitted

Takahashi, M. I., et al. 2006, ApJ, submitted

Taniguchi, Y., et al. 2005, JKAS, 38, 187

York, D. G., et al. 2000, AJ, 120, 1579

This preprint was prepared with the AAS LaTeX macros v5.2.

Table 1. Dithering offset for Pattern A

ID	ΔRA[a]	ΔDEC[b]	PA (deg)	ID	ΔRA[a]	ΔDEC[b]	PA (deg)
Pa01	45	31	0	La01	31	−45	90
Pa02	19	32	0	La02	32	−19	90
Pa03	−7	33	0	La03	33	7	90
Pa04	−33	31	0	La04	31	33	90
Pa05	46	−1	0	La05	−1	−46	90
Pa06	20	0	0	La06	0	−20	90
Pa07	−6	1	0	La07	1	6	90
Pa08	−32	−1	0	La08	−1	32	90
Pa09	45	−33	0	La09	−33	−45	90
Pa10	19	−32	0	La10	−32	−19	90
Pa11	−7	−31	0	La11	−31	7	90
Pa12	−33	−33	0	La12	−33	33	90
Pb01	32	33	0	Lb01	33	−32	90
Pb02	6	31	0	Lb02	31	−6	90
Pb03	−20	32	0	Lb03	32	20	90
Pb04	−46	33	0	Lb04	33	46	90
Pb05	33	1	0	Lb05	1	−33	90
Pb06	7	−1	0	Lb06	−1	−7	90
Pb07	−19	0	0	Lb07	0	19	90
Pb08	−45	1	0	Lb08	1	45	90
Pb09	32	−31	0	Lb09	−31	−32	90
Pb10	6	−33	0	Lb10	−33	−6	90
Pb11	−20	−32	0	Lb11	−32	20	90
Pb12	−46	−31	0	Lb12	−31	46	90

[a]Offset in RA from the COSMOS center position in units of arcmin.

[b]Offset in DEC from the COSMOS center position in units of arcmin.

Table 2. Dithering offset for Pattern C

ID	ΔRA[a]	ΔDEC[b]	PA (deg)	ID	ΔRA[a]	ΔDEC[b]	PA (deg)
A1	−3.5	26.5	0	C1	3.5	−26.5	0
A2	−30.5	27.5	0	C2	30.5	−27.5	0
A3	30.0	0.5	0	C3	−30.0	−0.5	0
A4	3.0	−0.5	0	C4	−3.0	0.5	0
A5	−3.5	−27.5	0	C5	3.5	27.5	0
A6	−30.5	−26.5	0	C6	30.5	26.5	0
A7	26.0	30.0	90	C7	−26.0	−30.0	90
A8	−27.0	3.0	90	C8	27.0	−3.0	90
A9	27.0	−30.0	90	C9	−27.0	30.0	90
B1	26.5	3.5	90	D1	−26.5	−3.5	90
B2	27.5	30.5	90	D2	−27.5	−30.5	90
B3	0.5	−30.0	90	D3	−0.5	30.0	90
B4	−0.5	−3.0	90	D4	0.5	3.0	90
B5	−27.5	3.5	90	D5	27.5	−3.5	90
B6	−26.5	30.5	90	D6	26.5	−30.5	90
B7	30.0	−26.0	0	D7	−30.0	26.0	0
B8	3.0	27.0	0	D8	−3.0	−27.0	0
B9	−30.0	−27.0	0	D9	30.0	27.0	0

[a]Offset in RA from the COSMOS center position in units of arcmin.

[b]Offset in DEC from the COSMOS center position in units of arcmin.

Table 3. A summary of observational programs

Semester	ID No.	PI	Program Title	Nights
S03B	239	Y. Taniguchi	COSMOS-Broad[a]	10
S04A	080	Y. Taniguchi	COSMOS-Narrow[b]	2.5
S04B	142	Y. Taniguchi	COSMOS-21[c]	8
S04B	UH-17A	N. Scoville	COSMOS-21[c]	4

[a]Suprime-Cam Imaging of the HST COSMOS 2-Degree ACS Survey Deep Field (Intensive Program).

[b]Wide-Field Search for Lyα Emitters at z=5.7 in the HST/COSMOS Field.

[c]COSMOS-21: Deep Intermediate & Narrow-band Survey of the COSMOS Field (Intensive Program). This proposal was also granted in S05B (S05B-013). However, this COSMOS-21 program will be described in a forthcoming paper.

Table 4. A summary of observational runs

ID No.	Period	Nights	Avail. Nights	Bands
S03B-239	2004 Jan 16-21	6	5	B, r', i', z'
S03B-239	2004 Feb 15-18	4	2	V, i'
S04A-080	2004 Apr 15-19[a]	2.5	1	$NB816$
S04B-142	2005 Jan 8-10	3	0	no obs.
UH-17A	2005 Feb 3	1	0	no obs.
S04B-142	2005 Feb 9-13	5	2	g', V, $NB816$
UH-17A	2005 Mar 10-12	3	1	$NB816$
S04B-142	2005 Apr 1-4[b]	4	3	g', $NB816$

[a]First half night was used in every night.

[b]Compensation nights because of the poor weather in S04B-142 Jan and Feb runs.

Table 5. A summary of the optical imaging data for COSMOS.

Band	λ_c[a] (Å)	$\Delta\lambda$[b] (Å)	Total TDT[c] (min)	$m_{\rm lim}$[d] (mag)	$m_{\rm lim}$[e] (mag)	$FWHM$(PSF)[f] ($''$)
B	4459.7	897	70.3	27.8	27.2	0.95
g'	4479.6	1265	86.0	27.2	26.6	1.58
V	5483.8	946	50.3	27.1	26.5	1.33
r'	6295.1	1382	36.0	27.2	26.6	1.05
i'	7640.8	1497	40.3	26.8	26.1	0.95
z'	9036.9	856	63.5	25.9	25.3	1.15
$NB816$	8151.0	117	187.7	26.1	25.7	1.51

[a]Central wavelength.

[b]Filter band width.

[c]The total target dedicated time.

[d]The 3σ limiting magnitude in the AB system within $2''$ diameter aperture.

[e]The 3σ limiting magnitude in the AB system within $3''$ diameter aperture.

[f]The PSF size of the final images. Note that the PSF size of each filter band is finally matched into $1\farcs6$ in the official photometric catalogue.

Table 6. SExtractor Parameters

Parameter	Setting	Comment
PARAMETERS_NAME	cosmos-subaru.param	Fields to be included in output catalog
FILTER_NAME	gauss_2.5_5x5.conv	Filter for detection image
STARNNW_NAME	default.nnw	Neural-Network_Weight table filename
CATALOG_NAME	STDOUT	Output to pipe instead of file
CATALOG_TYPE	ASCII	Output type
DETECT_TYPE	CCD	Detector type
DETECT_MINAREA	5	Minimum number of pixels above threshold
DETECT_THRESH	2	Detection Threshold in σ
ANALYSIS_THRESH	2	Limit for isophotal analysis σ
FILTER	Y	Use filtering
DEBLEND_NTHRESH	64	Number of deblending sub-thresholds
DEBLEND_MINCONT	0.0	Minimum contrast parameter for deblending
CLEAN	Y	Clean spurious detections
CLEAN_PARAM	1	Cleaning efficiency
MASK_TYPE	CORRECT	Correct flux for blended objects
PHOT_APERTURES	13.3, 20	MAG_APER aperture diameter(s) in pixels
PHOT_AUTOPARAMS	2.5, 3.5	MAG_AUTO parameters: <Kron_fact>,<min_radius>
PHOT_FLUXFRAC	0.2,0.5,0.8	Define n-light radii
PHOT_AUTOAPERS	20.0, 20.0	MAG_AUTO minimum apertures: estimation, photometry
SATUR_LEVEL	300000	Level of saturation
MAG_ZEROPOINT	31.4	Magnitude zero-point
GAIN	1	Gain is 1 for absolute RMS map
PIXEL_SCALE	0	Size of pixel in $''$
SEEING_FWHM	1.5	Stellar FWHM in $''$
BACK_SIZE	256	Background mesh in pixels
BACK_FILTERSIZE	5	Background filter
BACKPHOTO_TYPE	GLOBAL	Photometry background subtraction type
BACKPHOTO_THICK	8	Thickness of the background LOCAL annulus
WEIGHT_GAIN	N	Gain does not vary with changes in RMS noise
WEIGHT_TYPE	MAP_RMS	Set Weight image type
MEMORY_PIXSTACK	1000000	Number of pixels in stack
MEMORY_BUFSIZE	4096	Number of lines in buffer
MEMORY_OBJSTACK	60000	Size of the buffer containing objects

Table 6—Continued

Parameter	Setting	Comment
VERBOSE_TYPE	QUIET	

Table 7. Results of analysis for the detection completeness.

Band	Exponential Law[a]			de Vaucouleurs' Law[b]		
	95% (mag)	90% (mag)	50% (mag)	95% (mag)	90% (mag)	50% (mag)
B	24.1	24.7	25.5	24.1	24.7	25.3
g'	23.9	24.3	24.9	23.7	24.3	24.7
V	23.5	24.1	24.7	23.3	24.1	24.7
r'	23.5	24.1	24.7	23.3	23.7	24.7
i'	22.5	23.5	24.3	22.7	23.3	24.1
z'	22.1	22.9	23.3	22.1	22.7	23.1
$NB816$	22.1	23.1	23.7	22.1	22.9	23.5

[a]Magnitude at which the detection completeness is greater than 95%, 90%, and 50% for the model galaxies with the exponential light profile.

[b]Magnitude at which the detection completeness is greater than 95%, 90%, and 50% for the model galaxies with the de Vaucouleurs' law light profile.

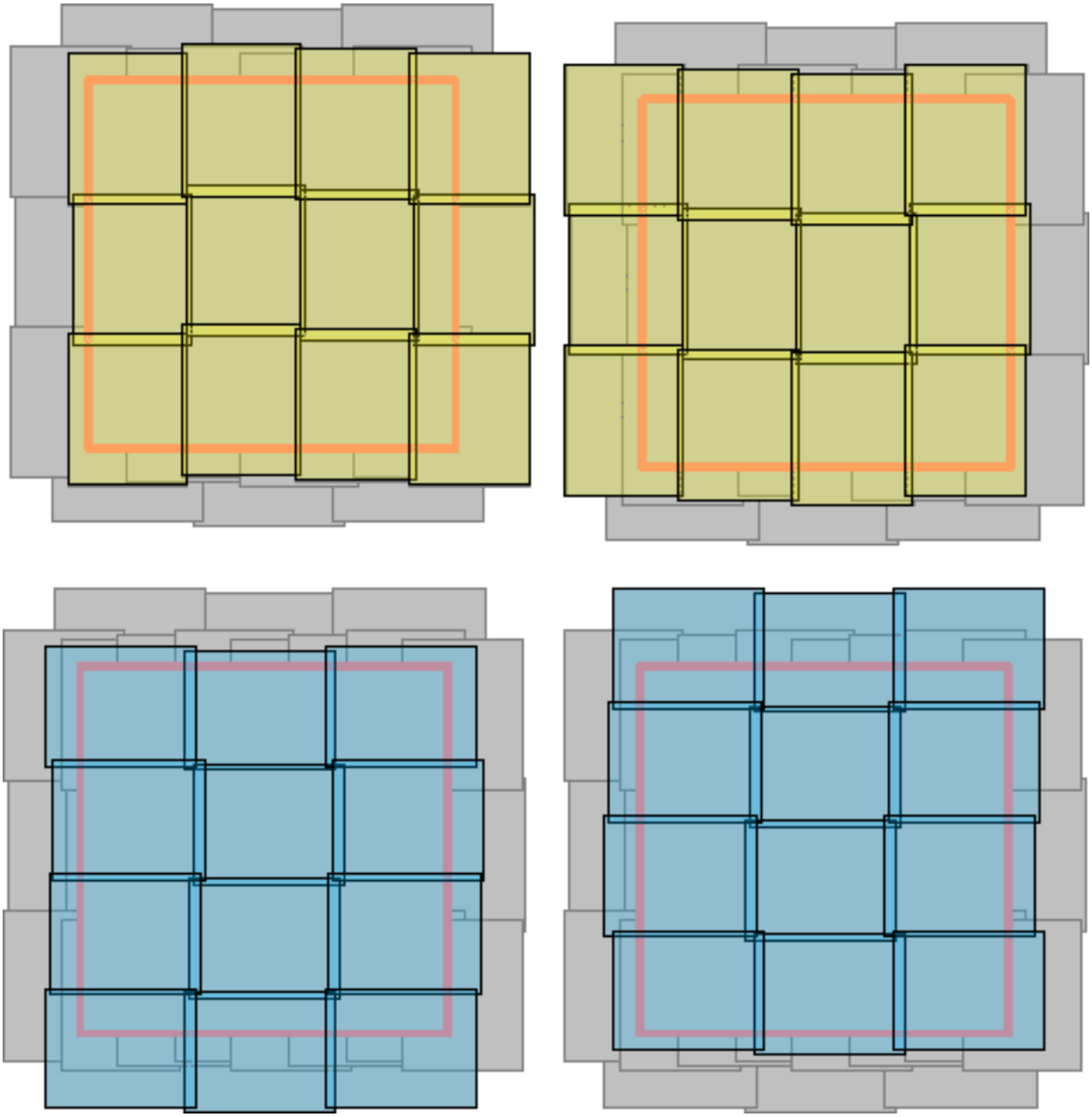

Fig. 1.— Dithering Pattern A.

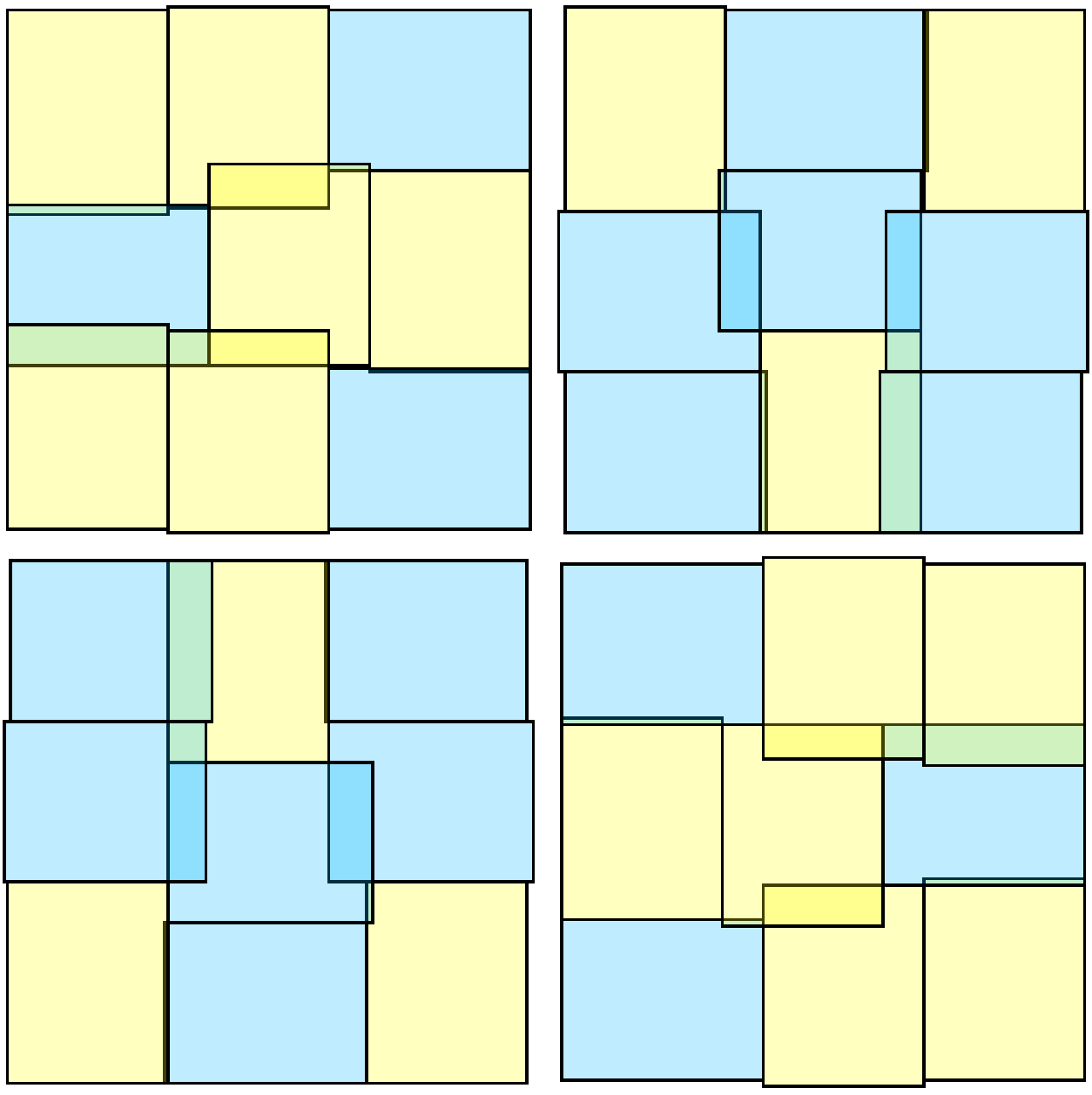

Fig. 2.— Dithering Pattern C.

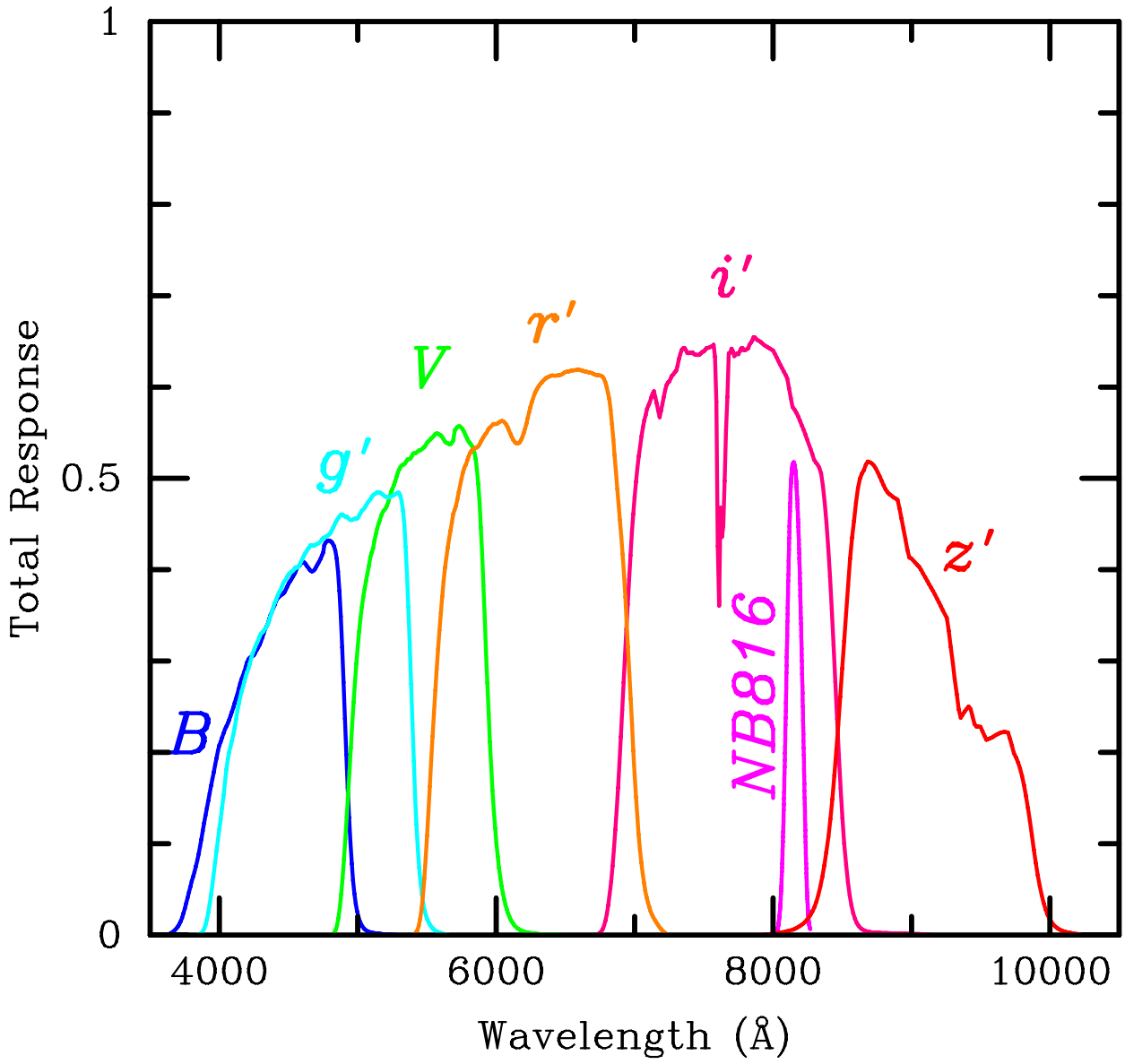

Fig. 3.— Filter response curves including the CCD sensitivity and the atmospheric transmission.

Fig. 4.— A color image of the COSMOS field made from B, r', and z' data. The image size is 1.5° × 1.5°.

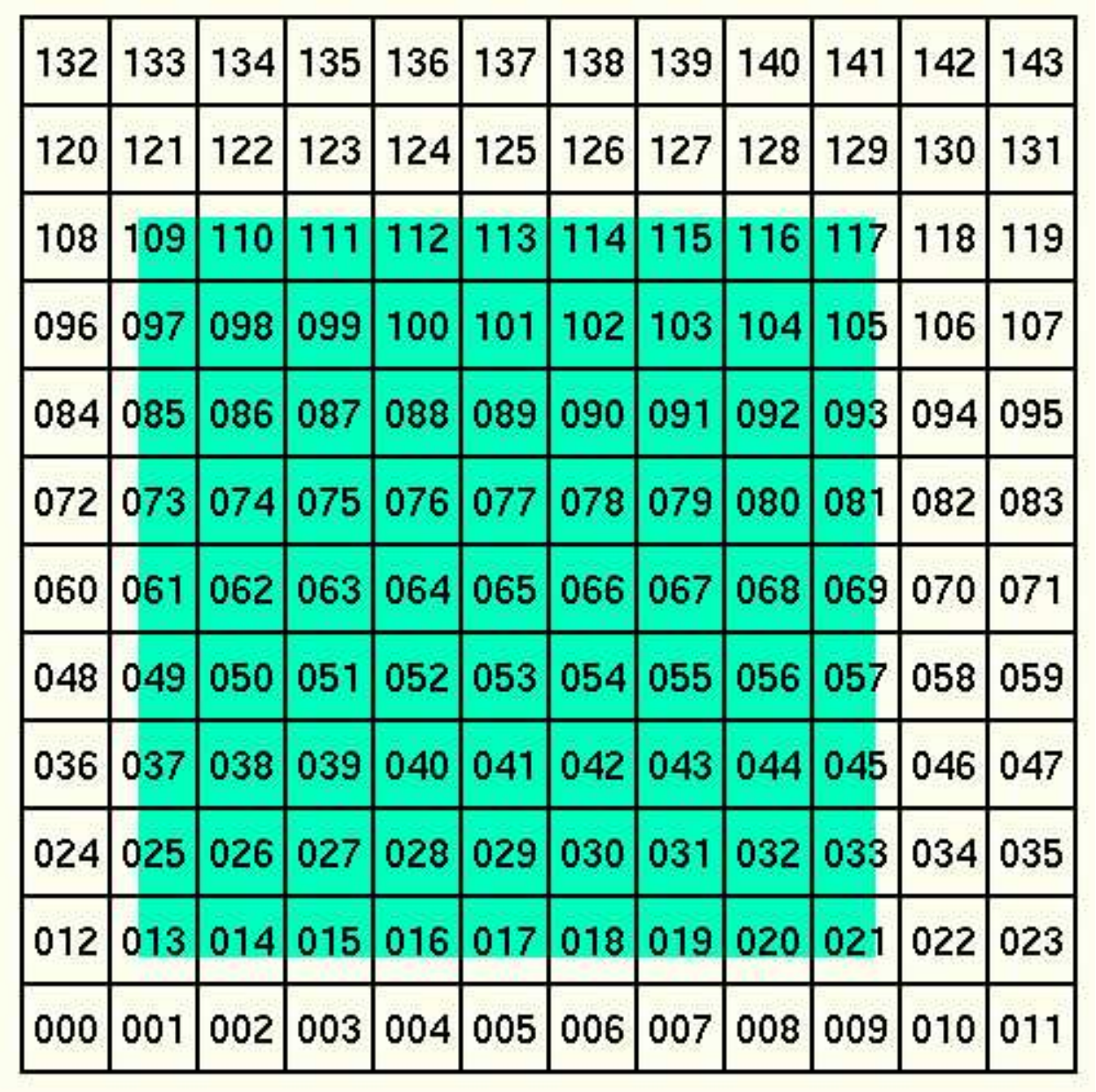

Fig. 5.— Sub-tiles of the reduced images. Each tile has a $10' \times 10'$ dimension. The region with light-blue color is the COSMOS 2 square degree field covered by our HST/ACS observations. The field center position is located at #65 tile.

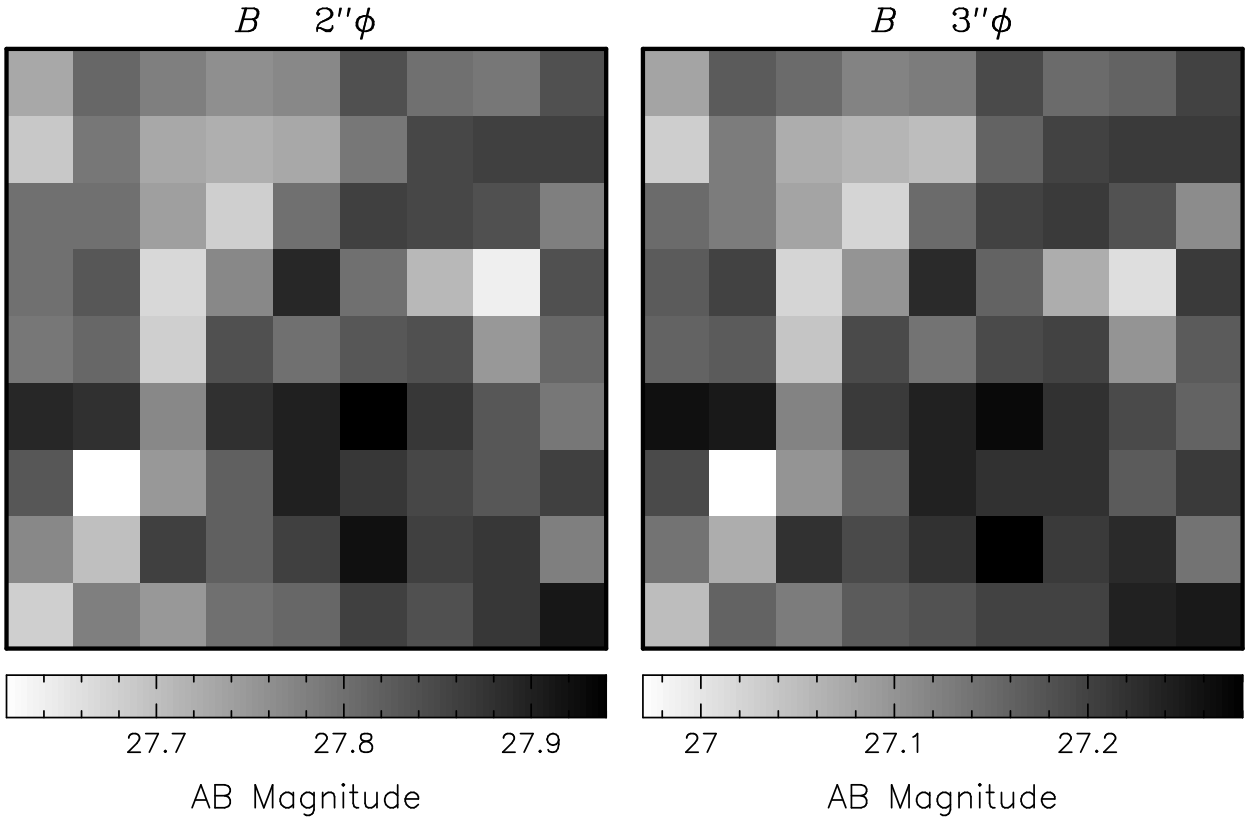

Fig. 6.— Variation of 3σ limiting magnitudes in the B band among the 81 tiles covering the COSMOS HST/ACS region (as shown by the region with light-blue color in Figure 5). The image size is $1.5^\circ \times 1.5^\circ$. The left panel shows the case for $2''$ diameter aperture and the right panel is for $3''$ diameter aperture.

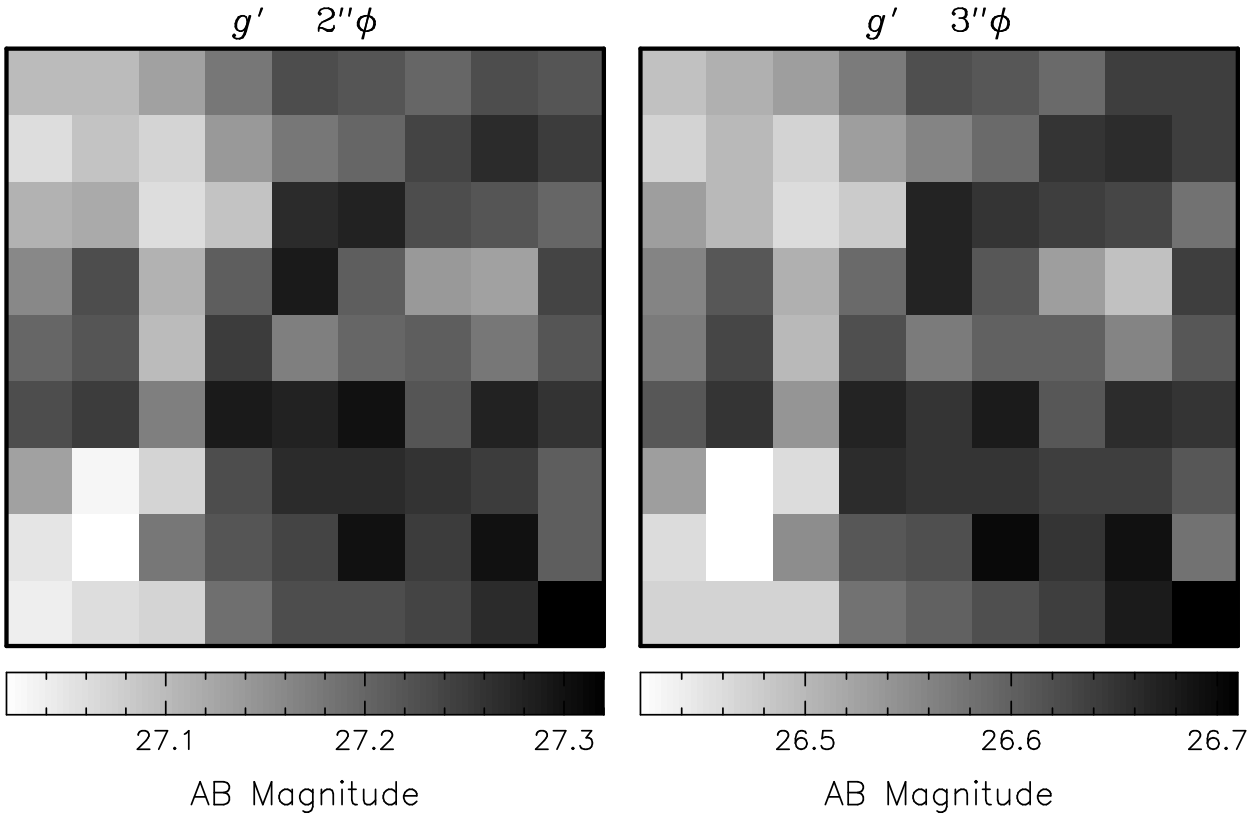

Fig. 7.— Same as Figure 6 for the g' band.

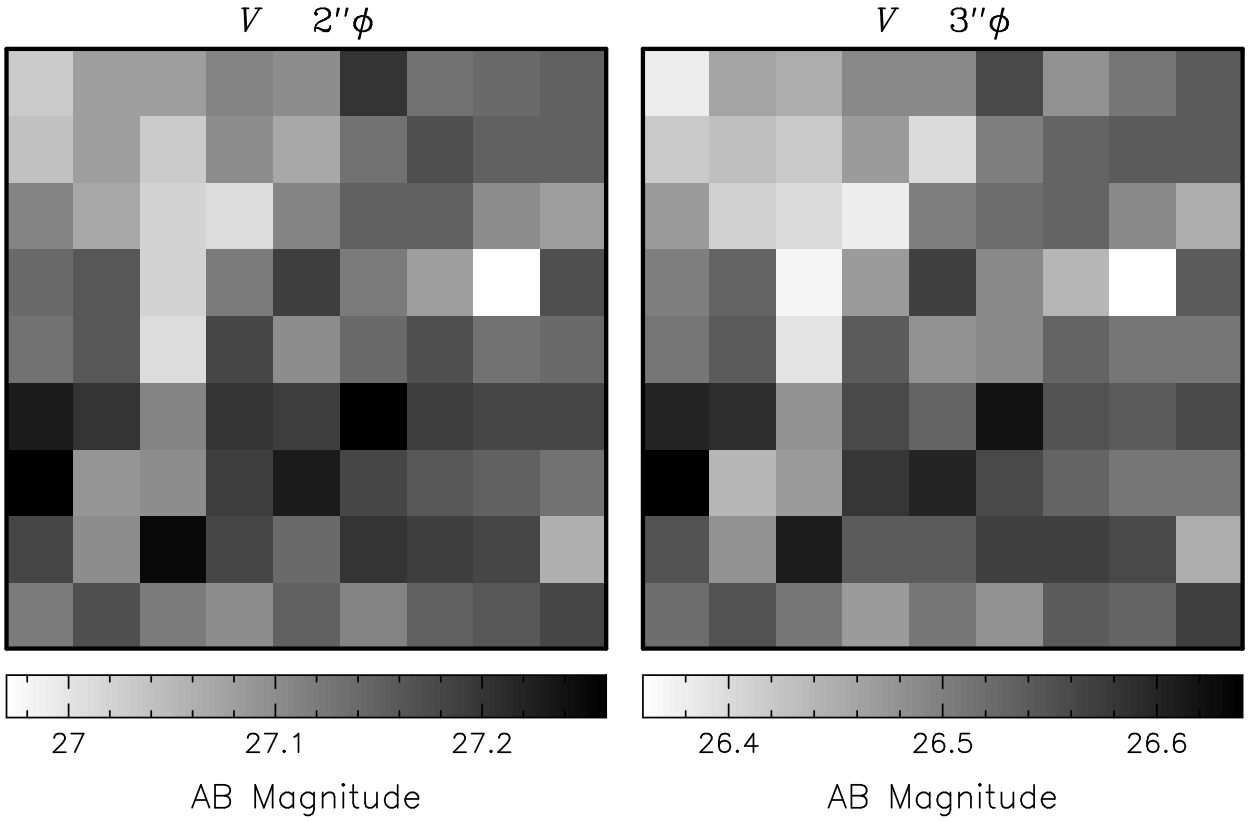

Fig. 8.— Same as Figure 6 for the V band.

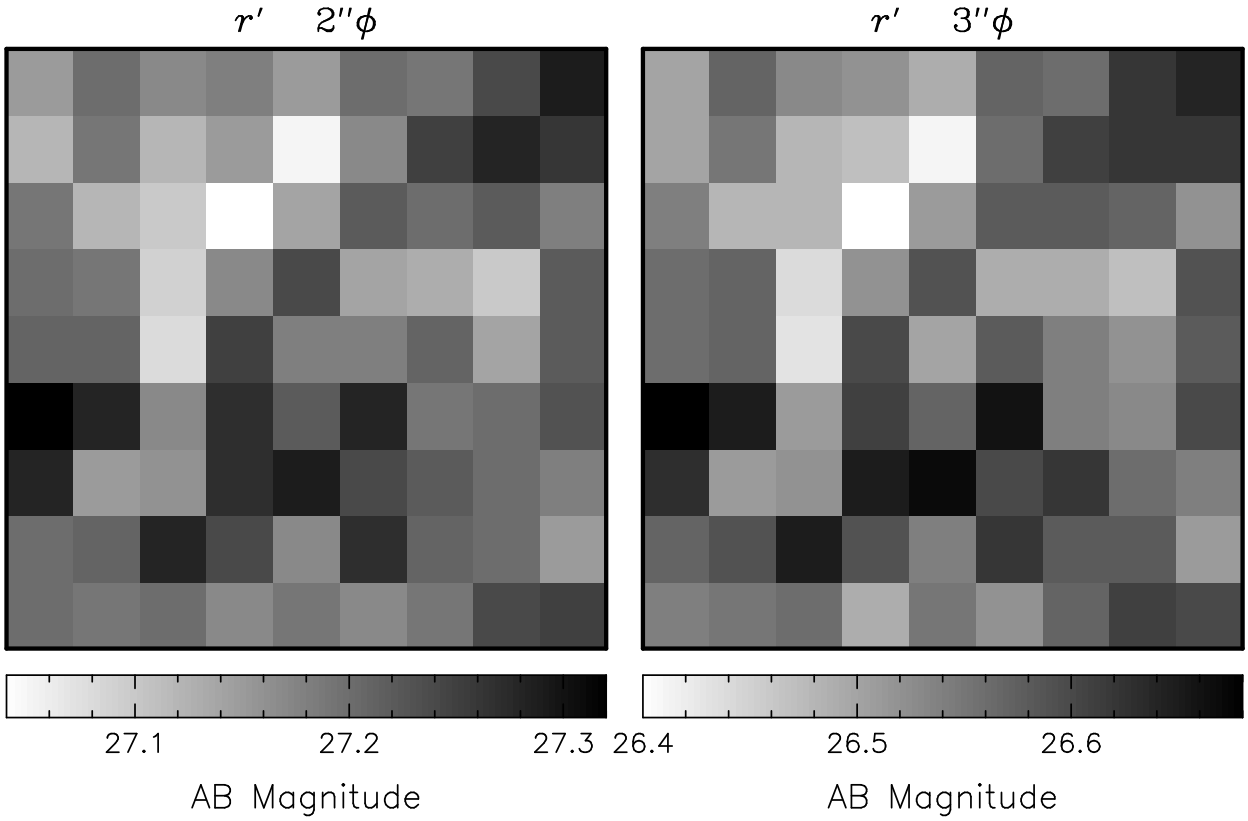

Fig. 9.— Same as Figure 6 for the r' band.

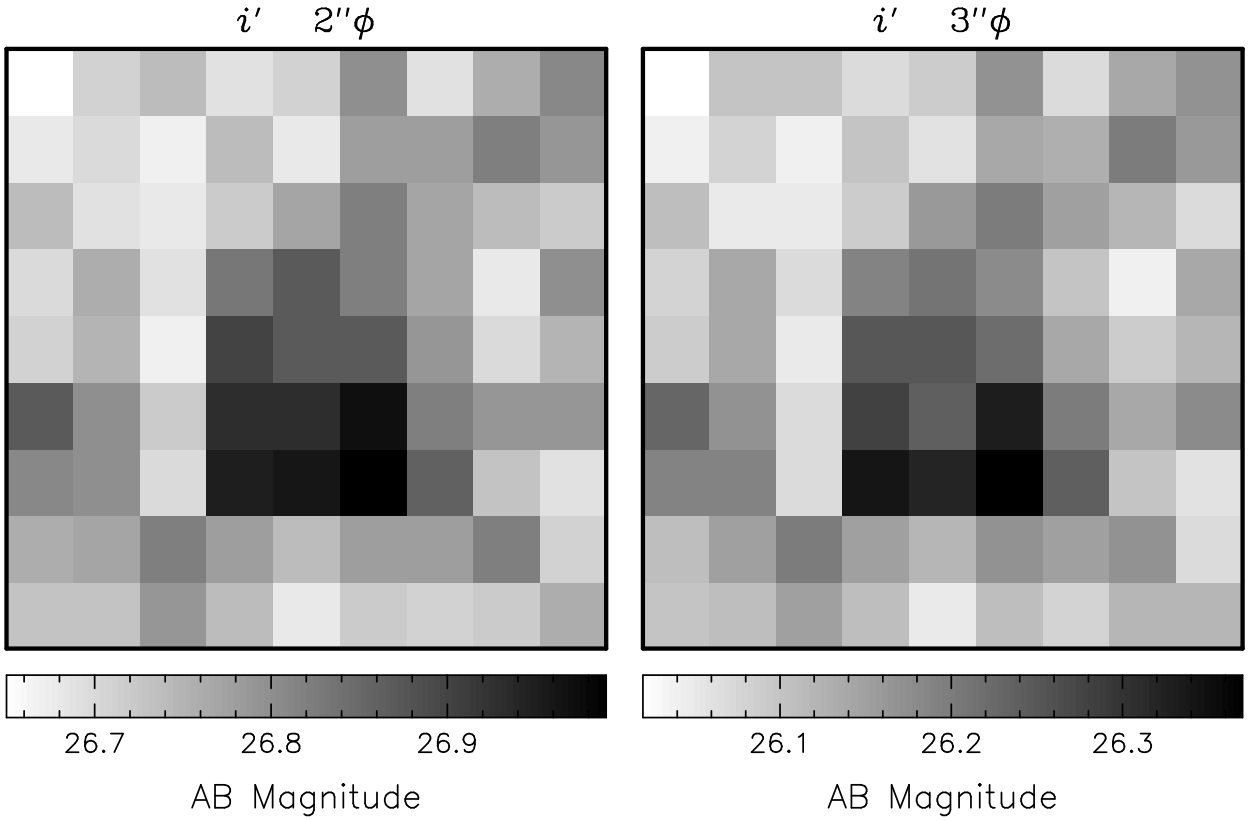

Fig. 10.— Same as Figure 6 for the i' band.

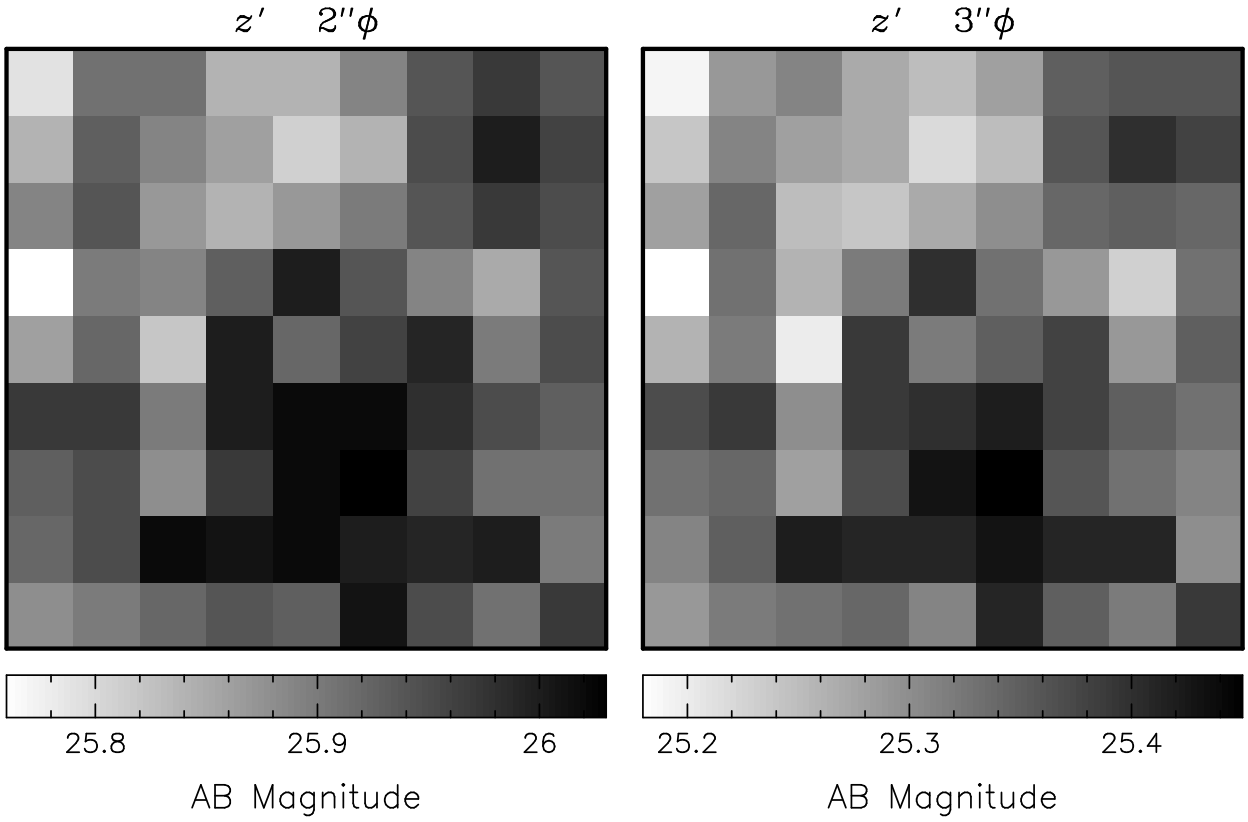

Fig. 11.— Same as Figure 6 for the z' band.

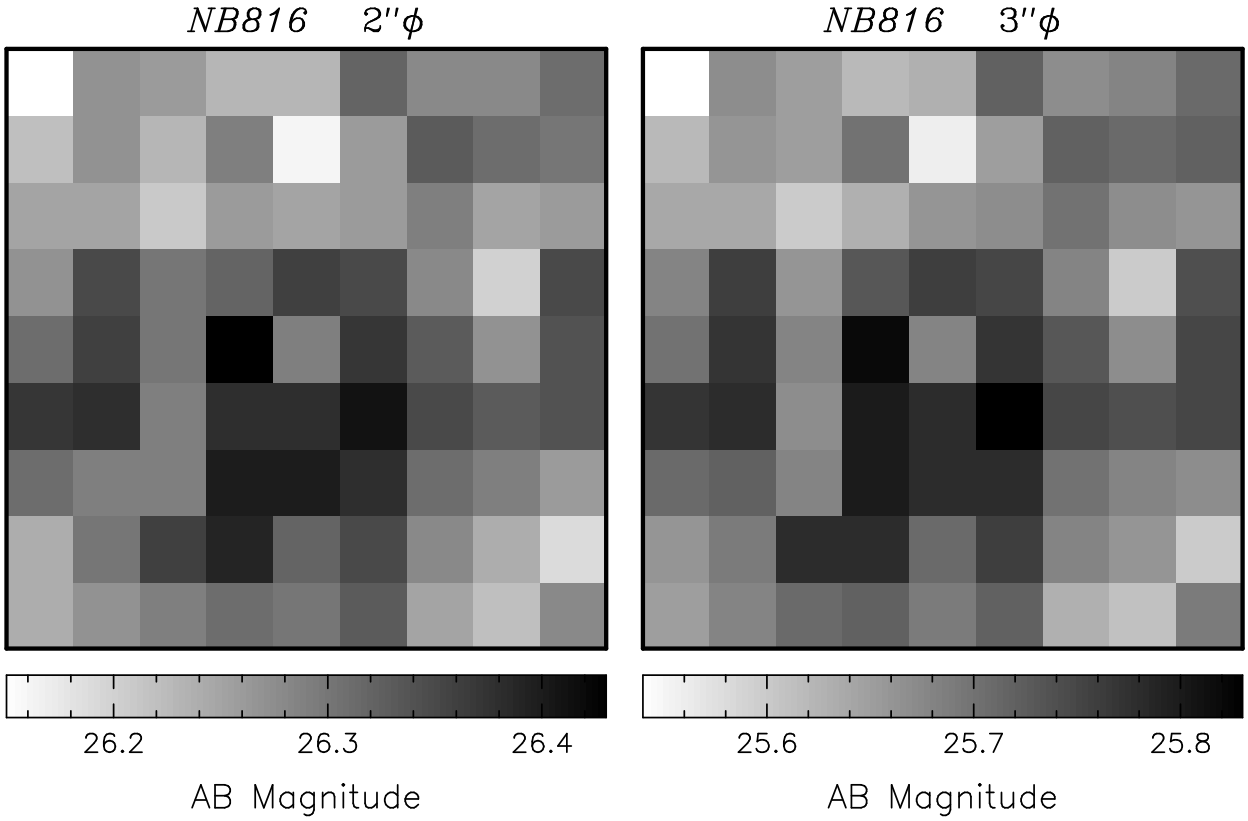

Fig. 12.— Same as Figure 6 for the $NB816$ band.

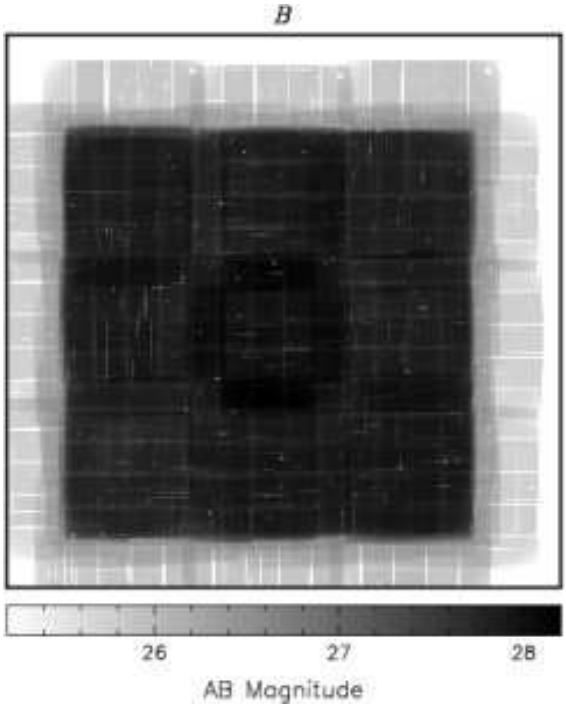

Fig. 13.— The map of 3σ limiting magnitude for $3''$ diameter aperture in the B band estimated by Capak et al. (2006a). The image size is $2^\circ \times 2^\circ$.

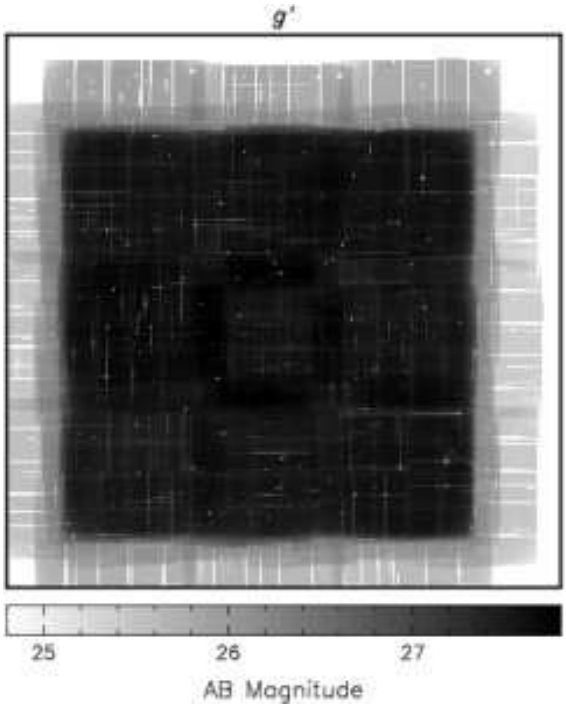

Fig. 14.— Same as Figure 13 for the g' band.

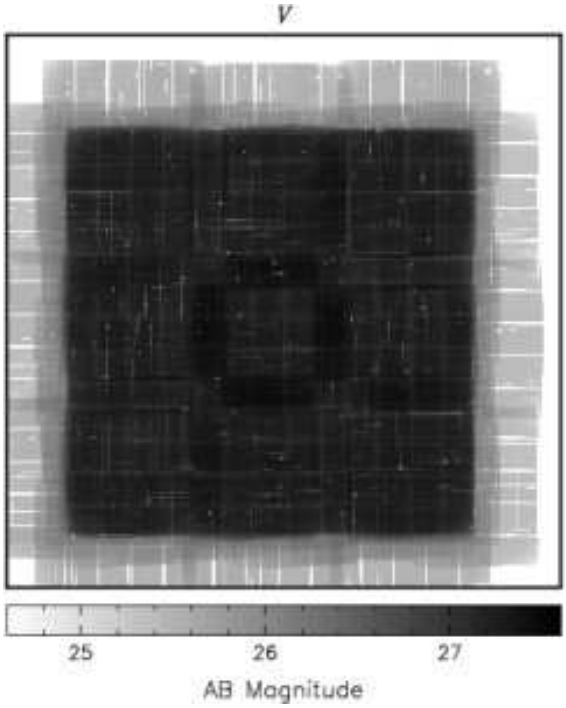

Fig. 15.— Same as Figure 13 for the V band.

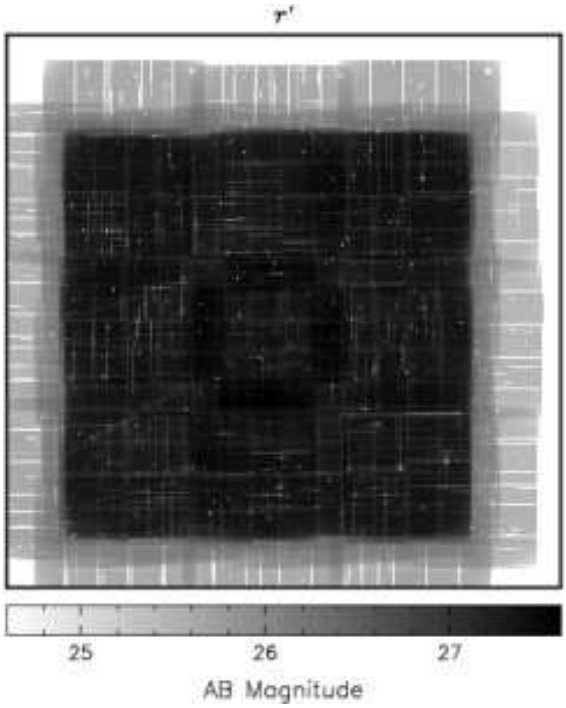

Fig. 16.— Same as Figure 13 for the r' band.

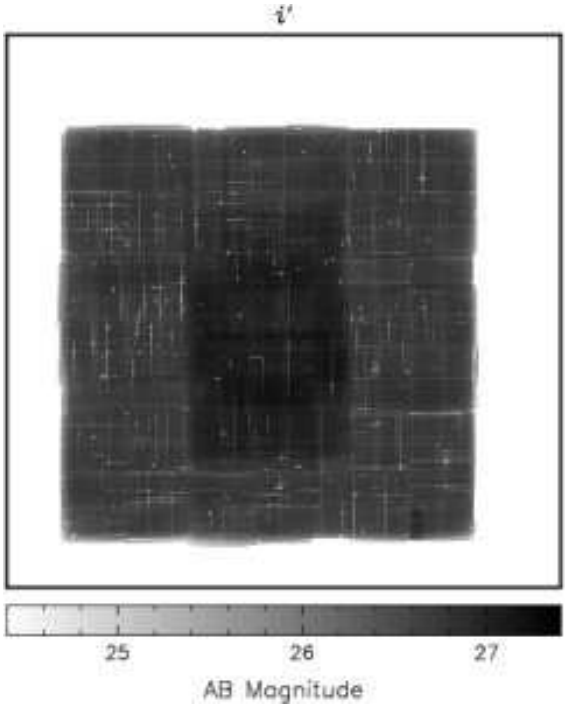

Fig. 17.— Same as Figure 13 for the i' band.

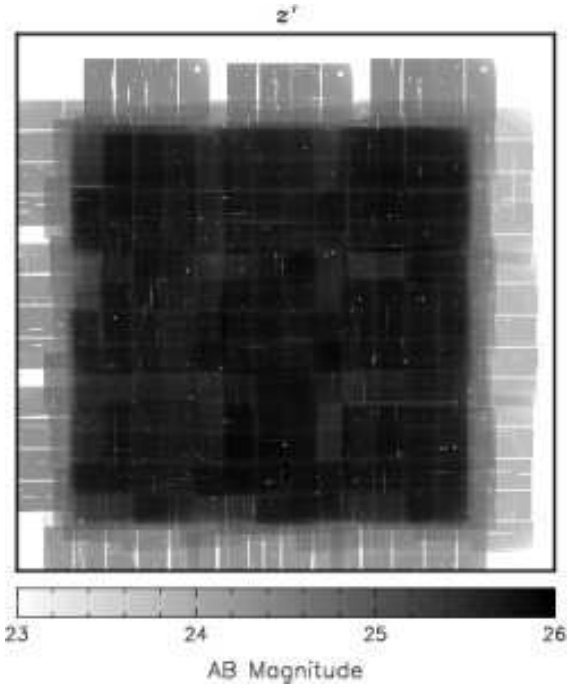

Fig. 18.— Same as Figure 13 for the z' band.

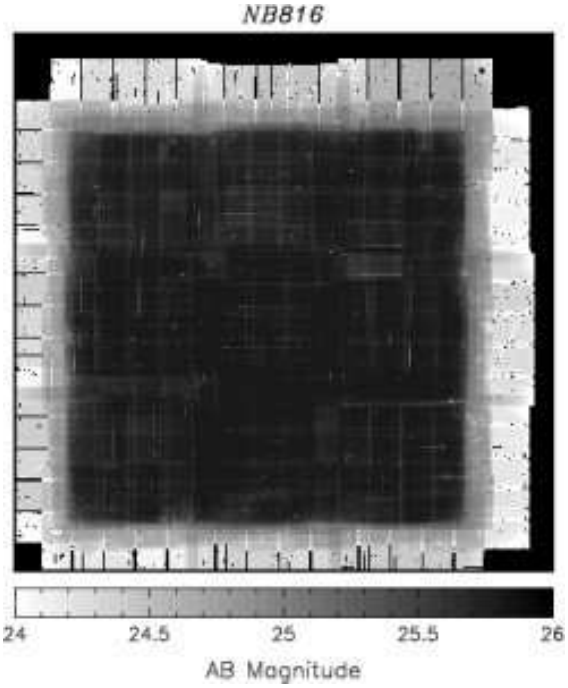

Fig. 19.— Same as Figure 13 for the $NB816$ band.

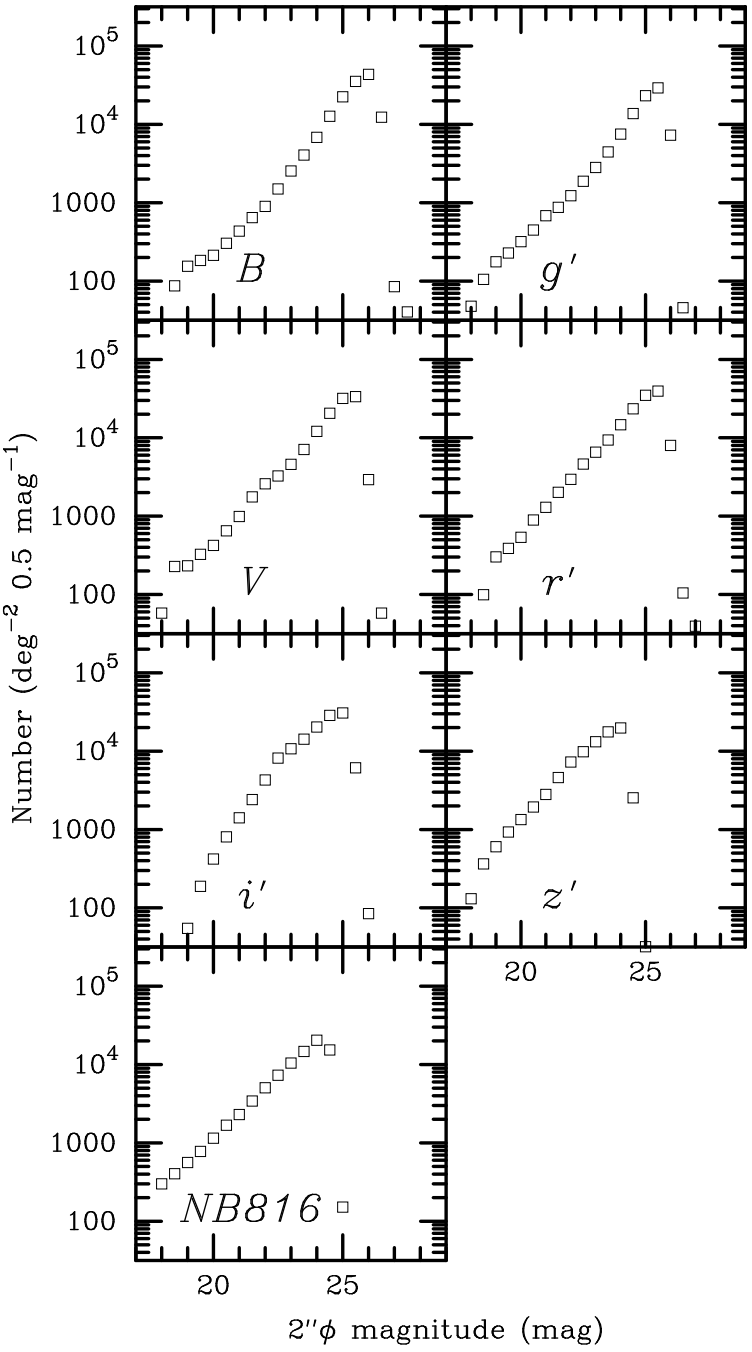

Fig. 20.— Number counts of the COSMOS field as a function of 2″ diameter magnitude.

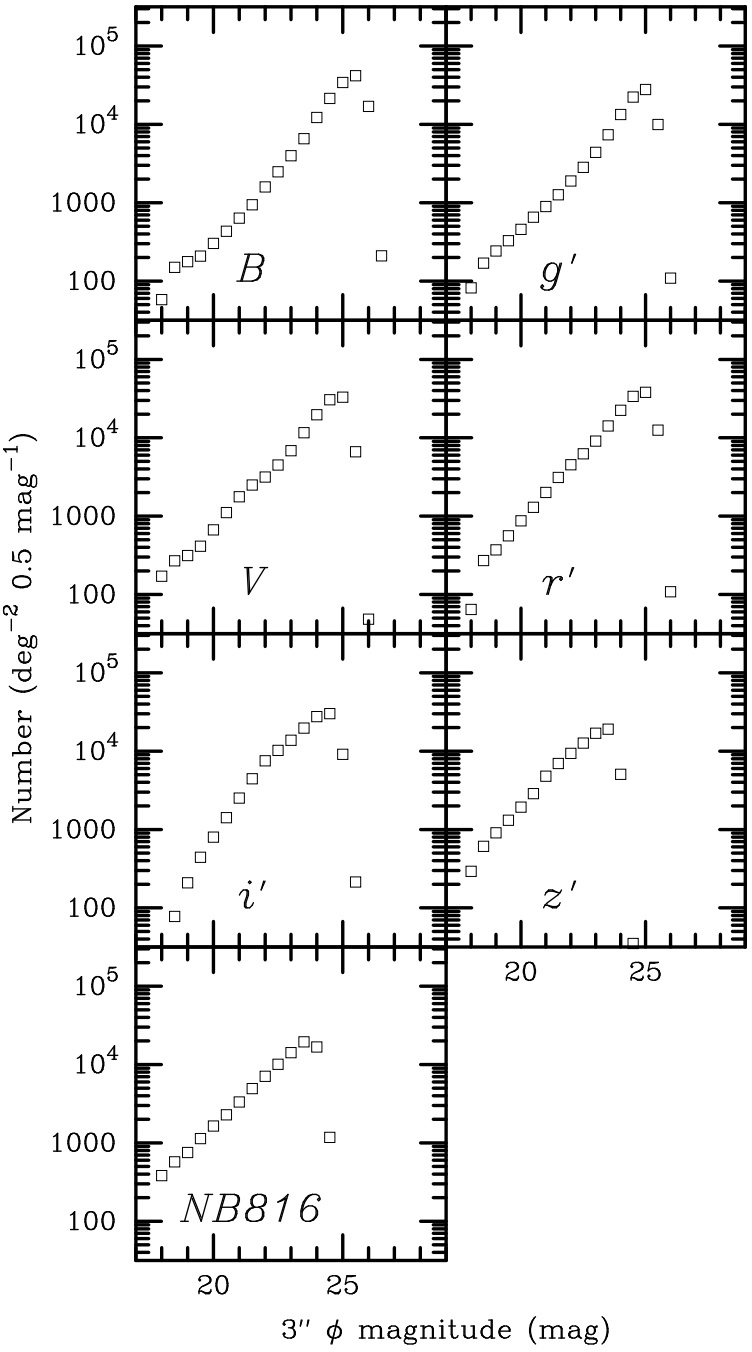

Fig. 21.— Number counts of the COSMOS field as a function of 3″ diameter magnitude.

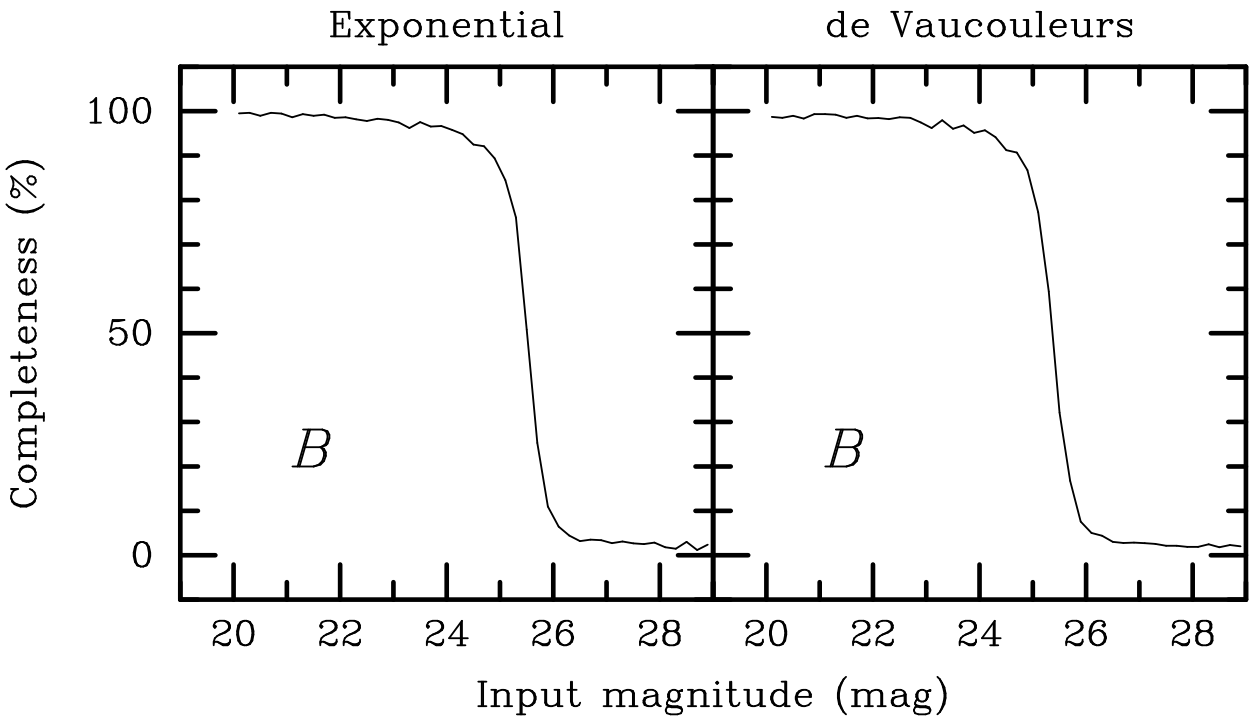

Fig. 22.— Detection completeness estimated by simulation in the B band as a function of input total magnitude of model galaxies. The left panel shows the case for model galaxies with the light profiles of the exponential law and the right panel shows the case for those with de Vaucouleurs' law profile.

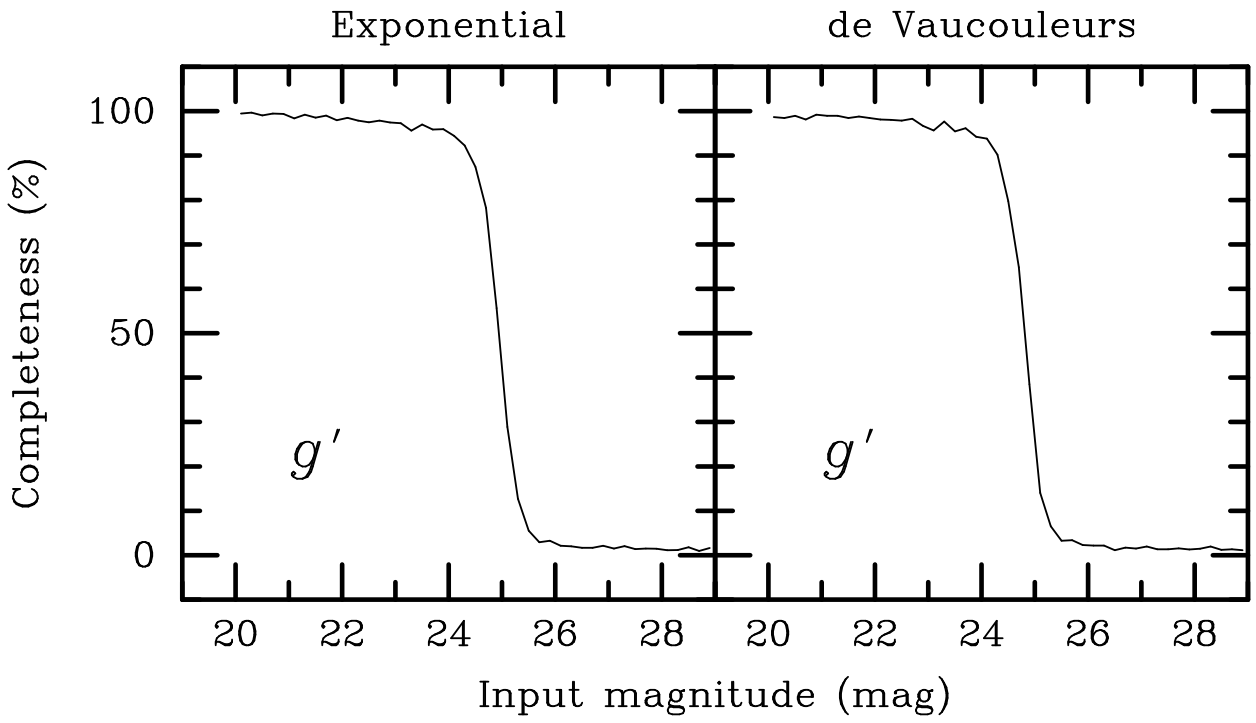

Fig. 23.— The same as Figure 22 but for the g' band.

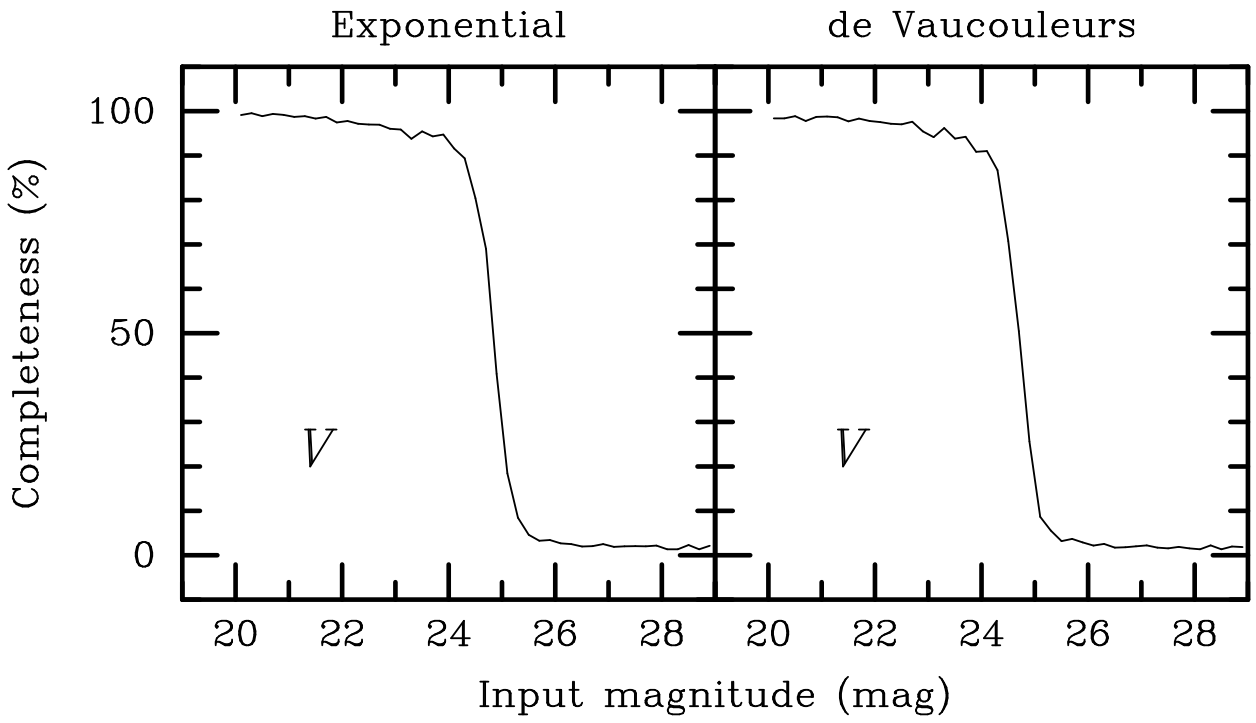

Fig. 24.— The same as Figure 22 but for the V band.

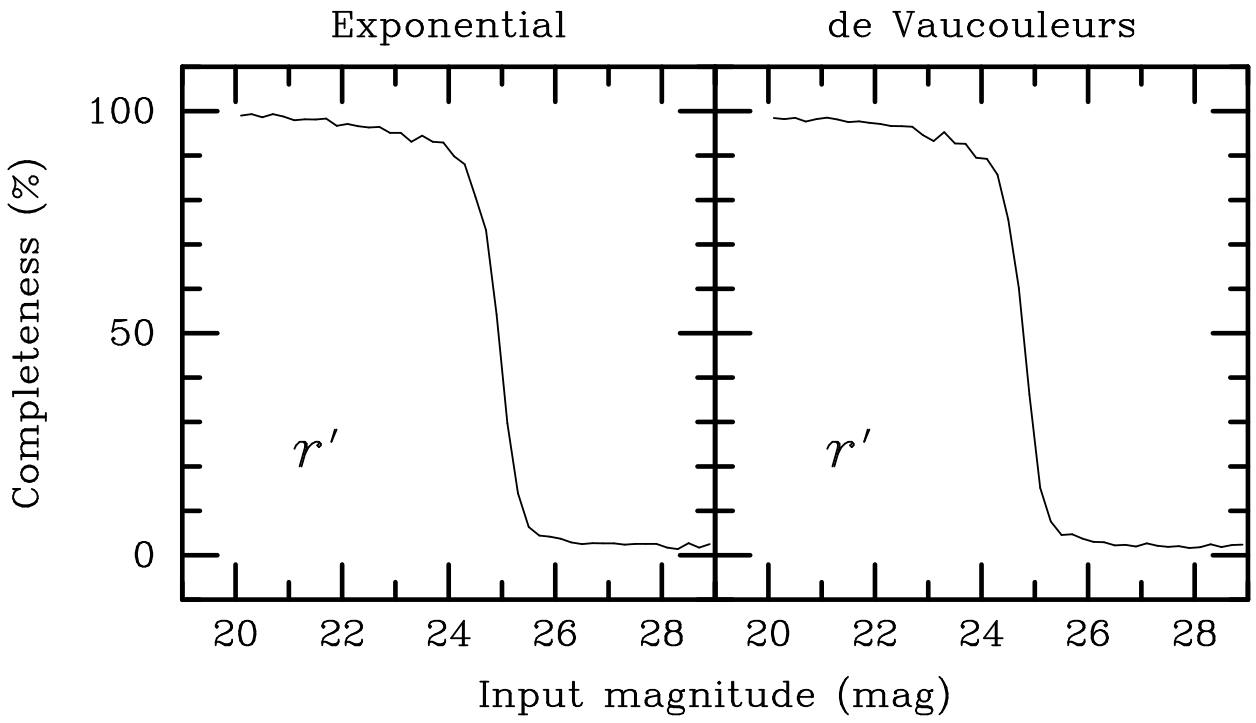

Fig. 25.— The same as Figure 22 but for the r' band.

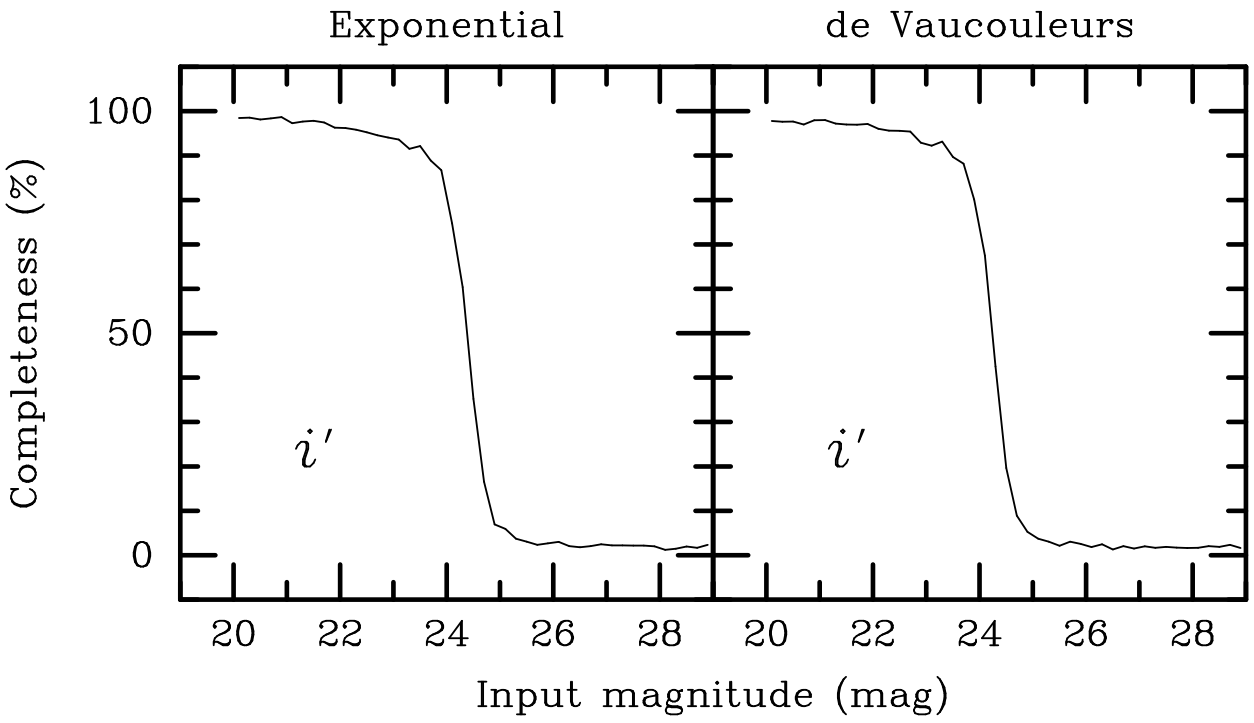

Fig. 26.— The same as Figure 22 but for the i' band.

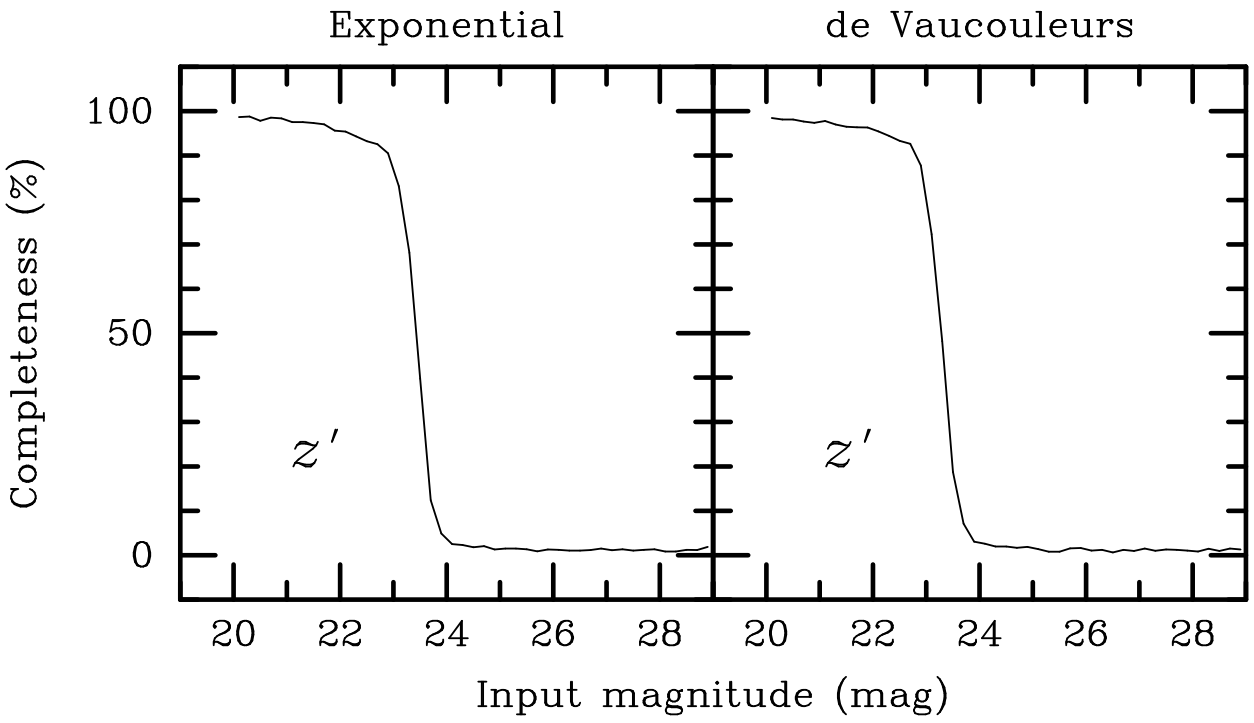

Fig. 27.— The same as Figure 22 but for the z' band.

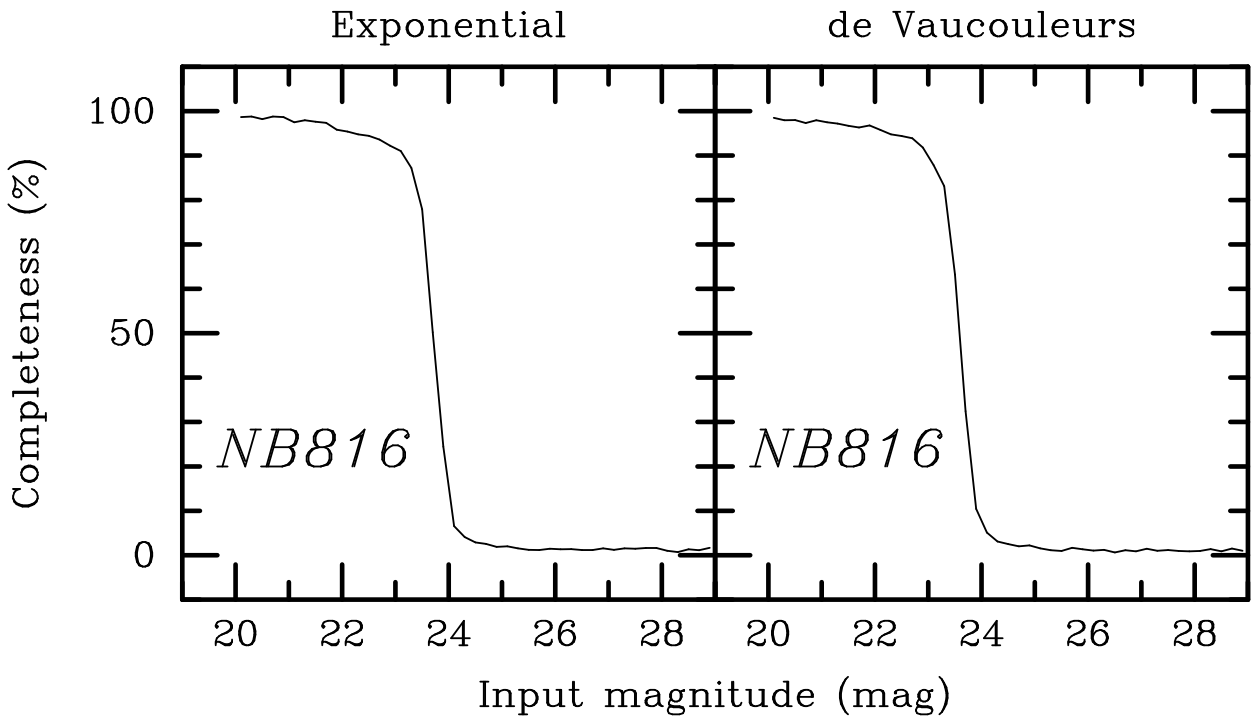

Fig. 28.— The same as Figure 22 but for the $NB816$ band.

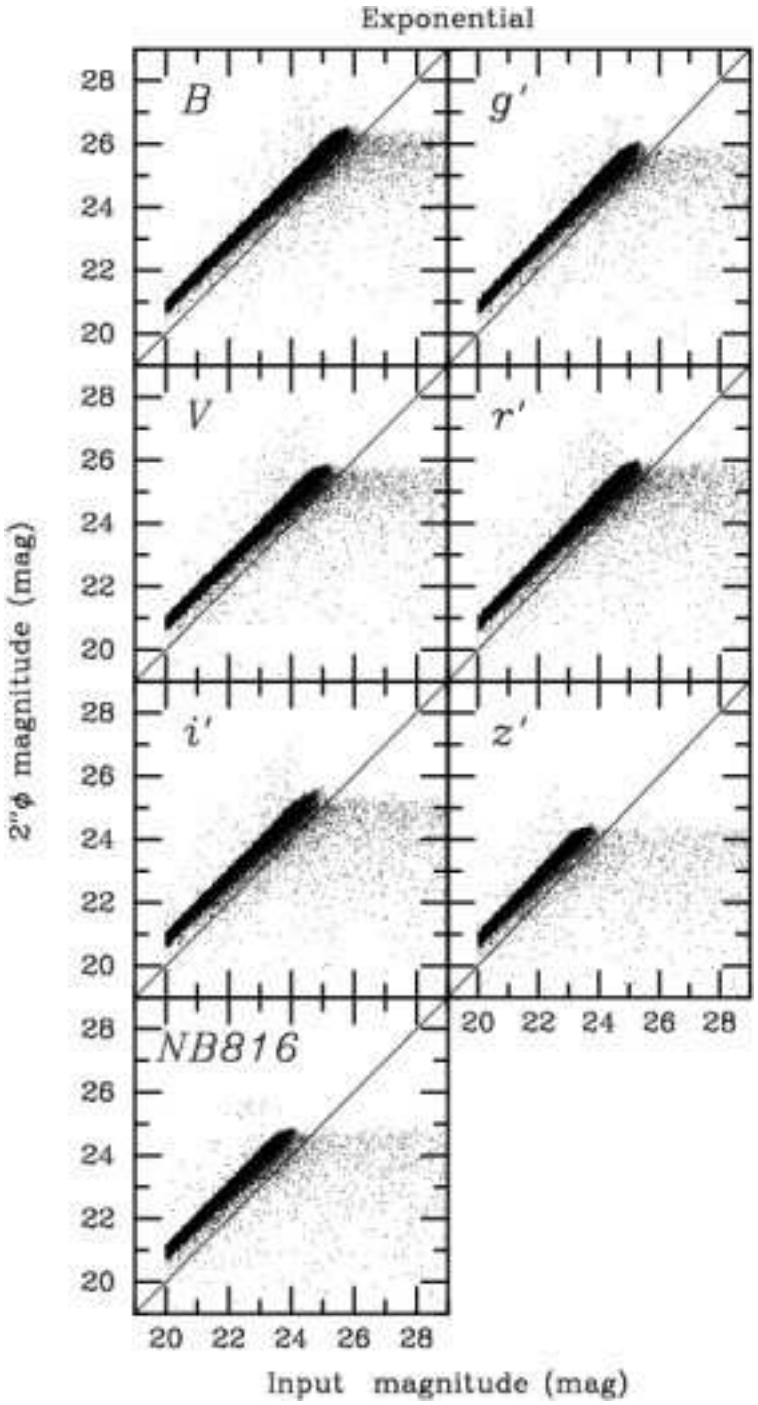

Fig. 29.— The relation between aperture magnitude of 2″ diameter and input total magnitude for the detected model galaxies with exponential profiles used in the completeness analysis.

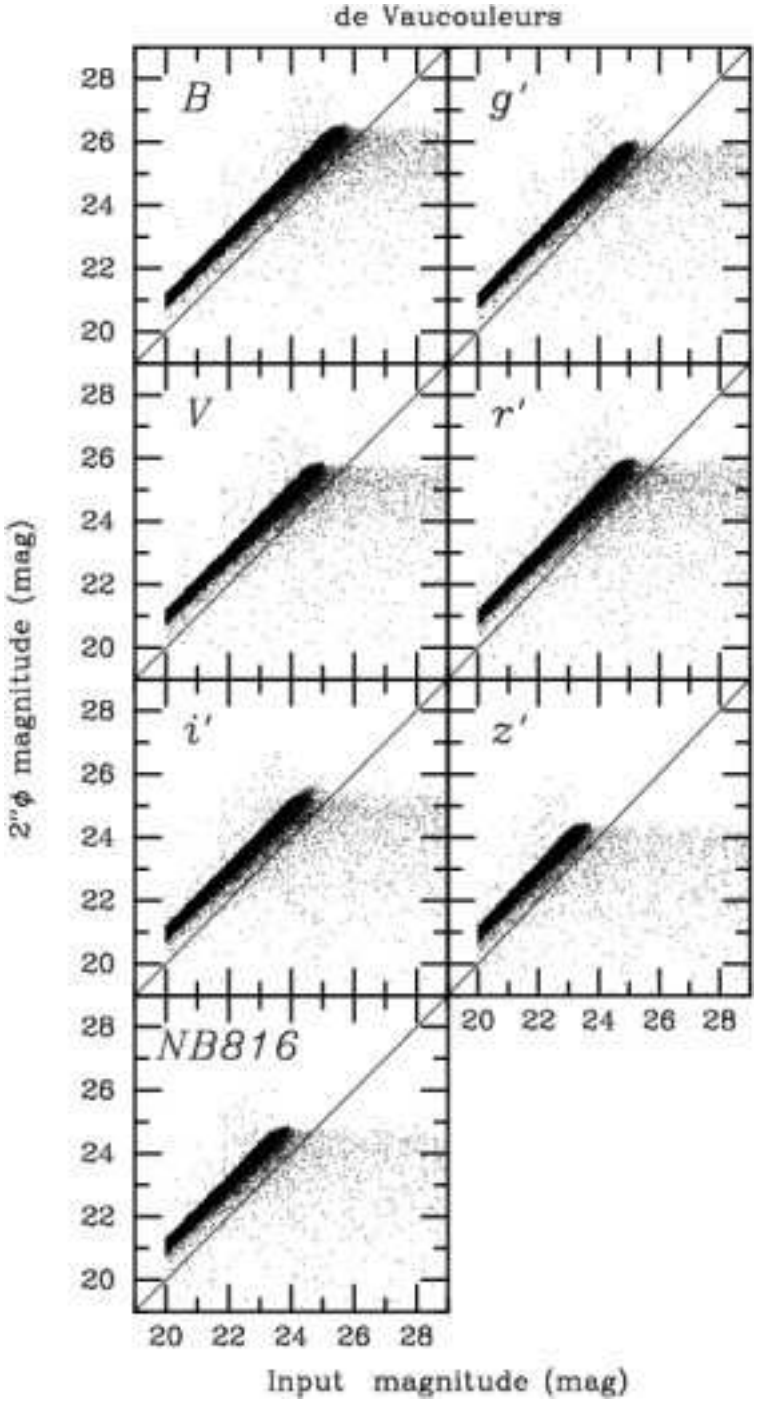

Fig. 30.— The relation between aperture magnitude of 2″ diameter and input total magnitude for the detected model galaxies with de Vaucouleurs' law profiles used in the completeness analysis.

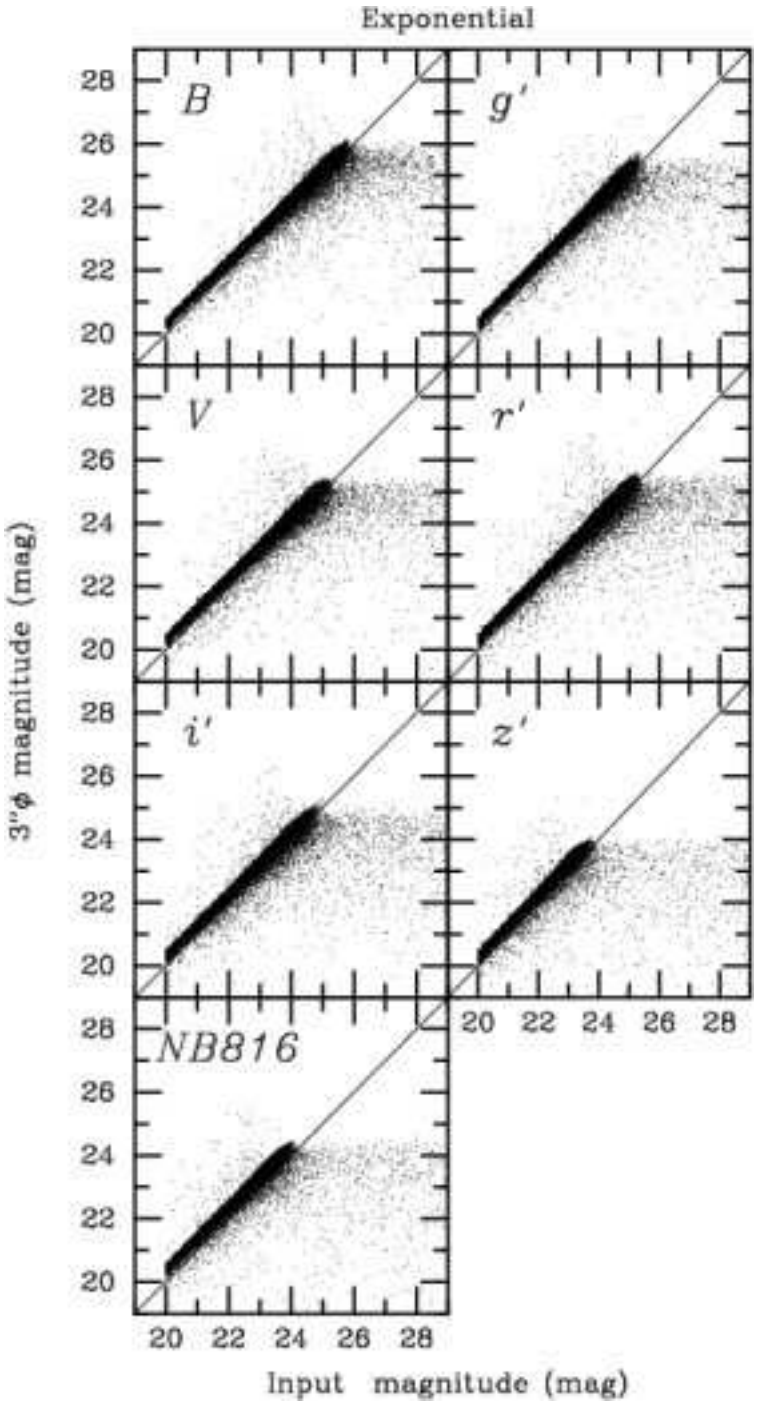

Fig. 31.— The relation between aperture magnitude of 3″ diameter and input total magnitude for the detected model galaxies with exponential profiles used in the completeness analysis.

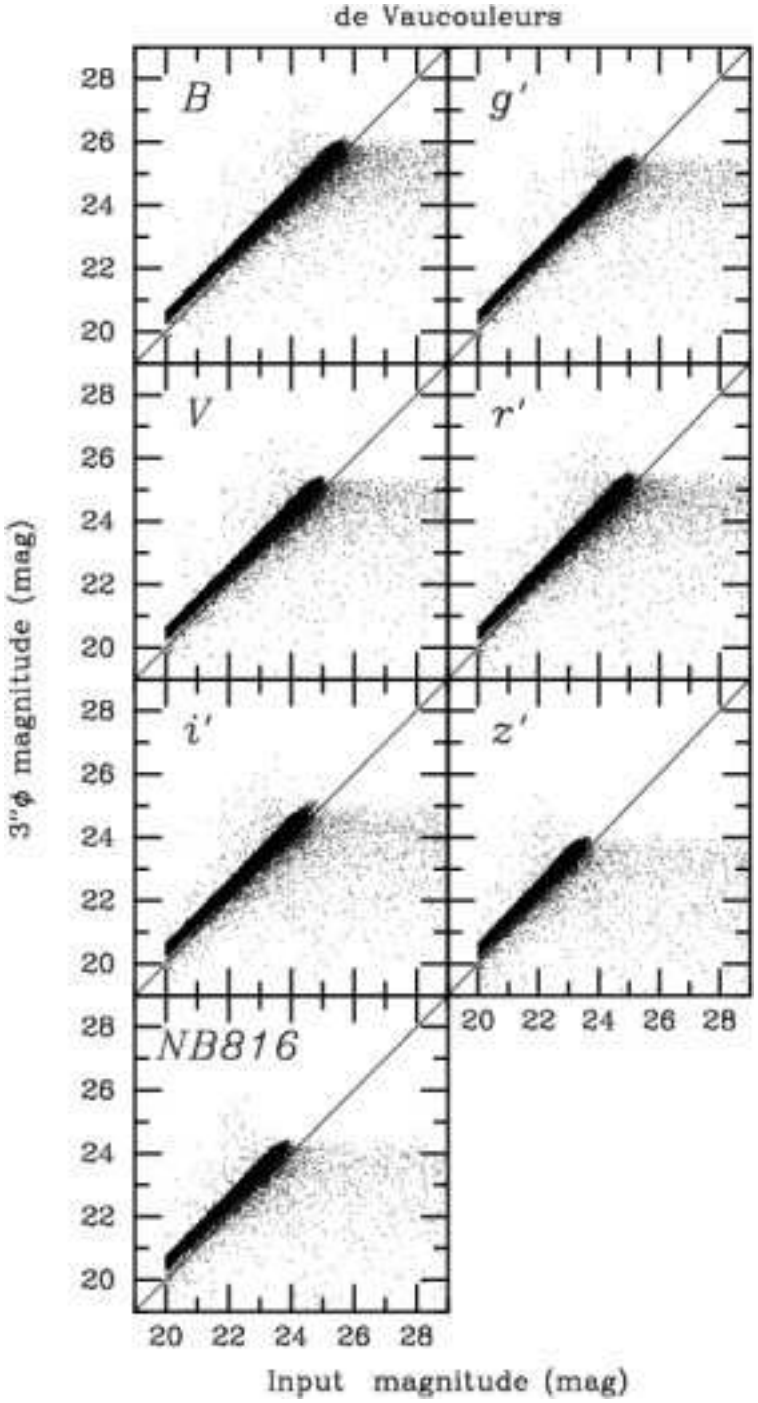

Fig. 32.— The relation between aperture magnitude of 3″ diameter and input total magnitude for the detected model galaxies with de Vaucouleurs' law profiles used in the completeness analysis.